Design and Implementation of a Thermal Hardware-in-the-Loop (THIL) Platform for Evaluating Physical Cooling Systems in Real-Time Simulation

by

Yin Fang

A Thesis Submitted to the Faculty of Graduate Studies of

The University of Manitoba

In partial fulfilment of the requirements of the degree of

MASTER OF SCIENCE

Department of Electrical and Computer Engineering

University of Manitoba

Winnipeg

Abstract

Power electronics (PE) take a critical role in electricity transformation, transmission and application in modern industrial utilization. Improving the efficiency while maintaining the stability of performance of electrical system and device is a continuously studied topic. In high power PE applications, hundreds and thousands of watts of heat is generated in conduction and switching status, as a result of that, design of cooling system is essential in a PE system design process.

This thesis proposed a real-time Thermal Hardware-In-the-Loop (THIL) simulation methodology to evaluate performance of cooling system of power semiconductors in a power circuit. This method required less energy and cost rather than traditional completely physical test as well as providing credible result of semiconductor junction temperature and instantaneous power dissipation.

Acknowledgments

Firstly, I would like to express the appreciation to my supervisor Prof. Carl Ho for his patient guidance and valuable academic knowledge throughout the master programme. Not only his personal wisdom and also the optimal life altitude gives a positive impact to my academic and further career life.

Secondly, graduated alumni Frank Xu and Isuru Jayawadana friendly and enthusiastic instruction when I began my research project as a new mentee. Their precious advice and effective tutorial greatly promotes my progress.

Finally, gratitude to my colleagues, Reza Eshkaftaki, Jalal Dadkhah and Avishek Ghosh in RIGA labs who provides meticulous help.

Dedication

To my parents and friends Chang Xu, Wei Jiang, Terulun and Jenny for their emotional support during this period.

Table of Contents

List of Tables

List of Figures

List of Abbreviations

AC	Alternating current
ADCs	Analog to digital converters
DACs	Digital to analog converters
DC	Direct current
IGBT	Insulated-gate bipolar transistor
Si	Silicon
SiC	Silicon Carbide
IC	Integrated circuit
USB	Universal Serial Bus
PC	Personal computer
PHIL	Power hardware in the loop
PI	Proportional-integral
PID	Proportional-integral-derivative
PWM	Pulse width modulation
VSC	Voltage source converters
MOSFET	Metal–oxide–semiconductor field-effect transistor
GaN	Gallium nitride
Hz	Hertz
PCB	Printed circuit boards
MMC	Modular multi-level converters

LUT	Look-up table
DPT	Double-pulse test
DUT	Device under test
HATTO	Hybrid Analytical Thermal Topology Optimization
FEA	Finite Element Analysis
HVDC	High-voltage direct current
GA	Genetic Algorithm
HTS	High-temperature superconductor
KEPCO	Korean Electric Power Corporation
TEM	Thermoelectric module
COP	Coefficient of performance
CPU	Central processing units
CFD	Computational Fluid Dynamics
LTS	Loop thermosyphon system
RSCAD	Real-Time Simulation Software
FPGA	Field Programmable Gate Arrays
MIPS	Millions of instructions per second
I/O	Input/output
ASIC	Application Specific Integrated Circuit
CPI	Cost-performance index

RC	Resistor-capacitor
VCVS	Voltage-controlled voltage source
GPAO	General purpose analogue output
GPAI	General purpose analogue input
SNR	Signal to Noise Ratio
CFD	computational fluid dynamics

Chapter 1 Introduction

1.1 Power Electronic Converters

1.1.1 Applications

Power electronic converters are fundamental components in electrical generation, transformation, and distribution and are widely used for domestic electronic devices and high-power industrial applications. The converters are designed to convert the electrical energy from one type to another, e.g., from alternating current (AC) to direct current (DC) and vice versa. DC-DC converters, which are used to regulate output voltage amplitude, are also widely used in the electrical system [1]- [3].

In recent decades, more and more studies come up to improve performance of converters including stabilities [4], power quality [5]-[6], and efficiency [7] while reducing cost [8] and power loss [9]. In order to achieve the mentioned enhancement, newly developed topologies and new materials are fabricated and evolved. Taking DC-DC regulators as an example, their critical sections are introduced with more detailed information in the next paragraph.

1.1.2 Critical Components in a DC-DC converter

A general introduction to the critical component of DC-DC regulators is presented in this subchapter, including typical topologies, controller strategies and choice of the controller chips, application of power semiconductors, and cooling systems.

A. Topologies

There are three basic topologies: buck, boost, and buck-boost in switched-mode DC-DC converters shown in Figure 1. Buck converters are referred as ‘step down’ converters which

means the output voltage is reduced rather than the input voltage [10]. Oppositely, boost converters are referred as ‘step up’ converters to provide higher voltage at the output terminal [11]. Finally, the buck-boost converter is able to step the output voltage up or down depending on the duty cycle of gate signal [12]. To achieve the target output of voltage or current of converters even experiencing fluctuations in input power source, controllers are necessary and fundamental in a converter design.

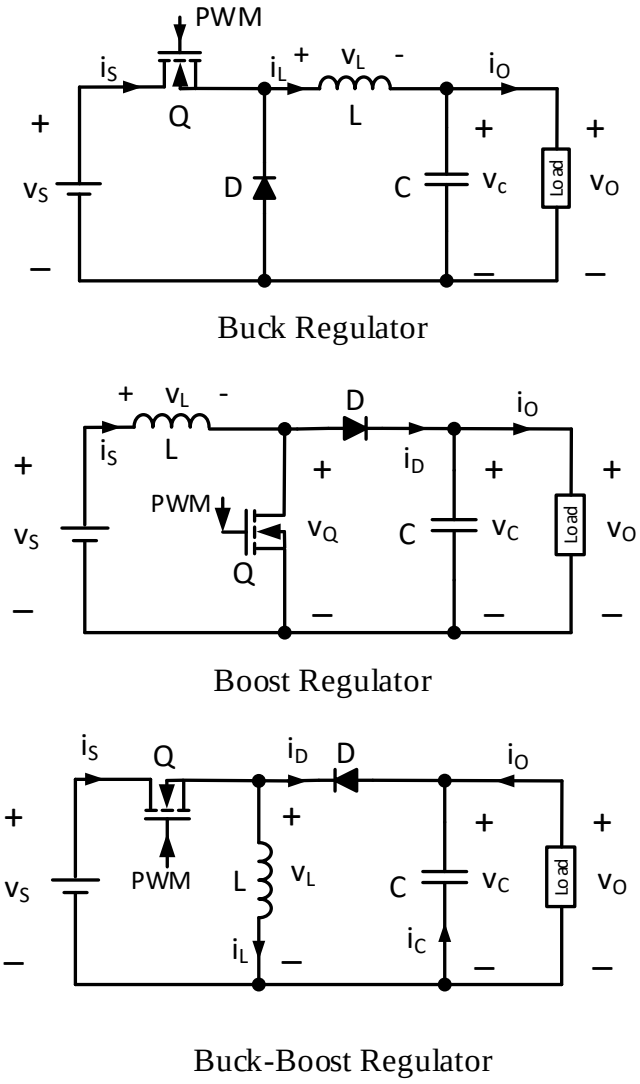

Figure 1 Typical topologies of switched-mode DC-DC regulators

B. Control Hardware

In order to provide a proper gate signal to the above converters, a controller is used to regulate the output voltage. Nowadays, digital control takes the advantage of fast dynamic response, comparatively less interface noise, and is much more commonly used in the modern electronics control strategy [13]. Although the information is lost in the process of sampling and finite quantization levels, this vanishment can be improved by increasing sampling frequency. Great developments in modern semiconductors make the clock frequency raising to 200k Hz for Digital Signal Processing (DSP) microcontrollers and 4000M Hz for Field Programmable Gate Arrays (FPGA).

For a digital controller, DSPs and FPGAs are commonly used for power electronic controllers [14]-[15]. Embedded function modules like analog-to-digital converter (ADC) and pulse width modulation (PWM) output make the microcontroller convenient to use in a system design. DSP is able to deal with complicated math processes, but the performance of microprocessors is limited by its system clock frequency. Oppositely, the FPGA consists of billions of gates that compose multiplier, register, and other high-level modules. The performance of FPGA is also limited by the number of gates. However, it is designed to manage tasks parallelly, which dramatically increases the number of millions of instructions per second (MIPS). Additionally, digital control is easier to manipulate, store and access measured data [16]. However, FPGA has a much higher cost rather than DSP. The comparison of DSP and FPGA is summarized in the table below:

Table 1 SUMMARY AND COMPARISON BETWEEN DSP AND FPGA

Functionality	DSP	FPGA
Programming Language	C language	Verilog hardware description language
System Clock Frequency	200M Hz	4000M Hz
Programming Software	Code Composer Studio	Quartus
Stability	Easier to encounter a system failure for interaction between tasks	More stable since the resources for individual tasks are independent
Cost	Relatively low	Relatively high

In all three types of basic switched mode DC-DC converter topologies, the passive electronic components are core factors to determine the steady-state large signal and ripples of output voltage and current. Besides that, the losses of semiconductor switch and diode are with critical influence for the system power efficiency. To satisfy the demand for higher power conversion and transformation, the switching frequency of converters raises to over 1M Hz [17]. Consequently, the switching loss increases markedly according to this ultra-high switching frequency.

1.1.3 Relationship Between Power Loss and Cooling Systems

The power loss is dissipated in the form of heat energy, as the result of that, the temperature of power semiconductors increases dramatically in a very short time. High temperature of the semiconductors can increase the risk to a higher power loss of the semiconductor and decrease in reliability, damage to semiconductor then leading open or short circuit problems and impacting the whole overall system [18]. By taking into consideration of these crucial effects, cooling systems are designed to dissipate the heat energy, then maintain the semiconductor temperature

within a proper range to achieve a safer operating region, longer lifetime, and higher efficiency of the overall converter system [19].

1.2 Power Semiconductors

1.2.1 Introduction of Types of Semiconductors

In a power electronic DC-DC converter, semiconductors, like Insulated-gate bipolar transistors (IGBT) [20], metal–oxide–semiconductor field-effect transistors (MOSFET) [21], play an important role for processing the power. Normally, an anti-parallel diode is applied with a MOSFET or an IGBT for protection purpose. Both IGBT and MOSFET are gate voltage-controlled devices. By applying required gate-to-source or gate-to-emitter voltage, the drain-to-source or collector-to-emitter terminals are forced to conduct.

Since the diode only allows the current to flow in one direction, it is commonly used in circuit design to regulate the polarization of current. Depending on the application for conduction like H-bridge circuits, or in high-frequency switched-mode converters, different materials of diodes are chosen to achieve lower conduction loss or switching loss.

Gallium Nitride (GaN) switches are popular choices in modern power electronic design. GaN switches take the advantage of lower switching loss of Wide-Bandgap (WBG) devices and now have an increasing market worldwide [22]-[23]. Silicon carbide (SiC) metal–oxide–semiconductor field-effect transistors (MOSFET) parallel with SiC Schottky diode is another widely used power semiconductor [24]. The SiC Schottky diodes have the benefit of small recovery loss which can lead to smaller power loss for diodes under high-frequency switching operations [25].

1.2.2 Introduction of Types of Semiconductor Power Loss

Semiconductor power loss can be classified into two main types of loss: conduction loss and switching loss. Firstly, the conduction loss is generated during the period when the semiconductor is in conduction. Secondly, switching loss is produced during the switching transient, including (1) recovery loss of diode, (2) switching-on loss, and (3) switching-off loss of IGBTs or MOSFETs. Both two types of power loss can be estimated by solving the mathematical integration analytically and measuring the current waveform quantitively [26].

Generally, the device capacitance dominates the maximum limitation of switching frequency [27]. Consequently, the drawback of SiC MOSFET is its higher capacitance capacity than planar silicon MOSFET. To overcome the capacitance, a large current density is required in SiC MOSFET components which implies that the on-resistance need to be small enough to reduce the conduction loss. The above reasons make SiC MOSFETs design focus on minimizing on-resistance and device capacitance and optimizing the power semiconductor performance [28].

Additionally, the switching power loss is also easily affected by other unavoidable factors like parasitic inductance [29]. Greater parasitic inductance including loop inductance, wire inductance, and leg inductance between the semiconductors metal connection and printed circuit boards (PCB) increases the turn-on and turn-off loss of the IGBT. The loop inductance on the emitter of IGBT has a considerable impact on the gate driver circuit since it is involved in both gate driver and power circuit [30].

Furthermore, higher switching frequency generally introduces larger switching loss as well as the conduction loss decreases. Appropriate components selection relies on the implementation

of semiconductors and balance between switching loss and conduction loss in each specific case. These are the key factors considered to achieve higher efficiency in the design process.

1.2.3 Methodologies to Determine Semiconductor Loss

Appropriate estimation of the semiconductor power loss provides essential information for further application design. In the past decades, diverse methods are created to assess real-time power loss with increasing accuracy.

Estimation of semiconductor power loss is a critical factor while predicting the efficiency and lifetime of power converters. However, it can be affected by many reasons, for example, converter switching frequency, maximum allowable ambient temperature [31], forward current of diode, collector-emitter voltage drop, gate-emitter voltage drop for IGBT, etc. Literature [32] suggests that implementing a look-up table (LUT) which contains the IGBT and diode conduction and switching energy loss information. By inputting the measured operating current, estimated case temperature, and the DC voltage level, the power loss is located in the LUT. This method in high-speed simulation software can significantly decrease the simulation time and give a sufficiently accurate result after combining it with the ideal component model. Another suggestion in literature [33] is detecting the change of current in switching transient as the current slope to calculate the recovery loss of the diode. Measurements are required to determine the semiconductor power loss of a high-frequency switch-mode converter.

Double-pulse test (DPT) is prominent for determining the switching performance of the switching cell which consists of a diode, a switch, a current source, and a voltage source [34]. The current source can be represented by an inductor, and the voltage source can be replaced by a capacitor. As shown in Figure 2, a conventional double-pulse test consists of two cascaded IGBTs

with two anti-parallel diodes in series with a voltage source and an inductor in parallel with the upper-located IGBT. The lower IGBT (T2) and upper anti-parallel freewheeling diode (D1) constitute a switching cell which is the device under test in this case. By applying two pulses with identified delay to the gate terminal of the lower IGBT, the DPT is established. The first pulse is targeted to charge up the current in the load inductor to the desired value and record the switching-off characteristic when turning it off. Then, the following delay is aimed to maintain the inductor current while letting it flow through the high-side diode (D1) and form a freewheeling current. Finally, the lower side IGBT (T2) is forced on again and the switching-on characteristic and freewheeling diode recovery loss are recorded [35]. Another topology of the circuit in Figure 3 is suggested to apply an H-bridge circuit to perform the DPT to achieve a switching performance that is closer to practical implementation which improves the accuracy of estimation of semiconductor power loss [36]-[37]. Based on the results of estimation or measurements, a LUT can be created including the conditions of volts, currents and temperature.

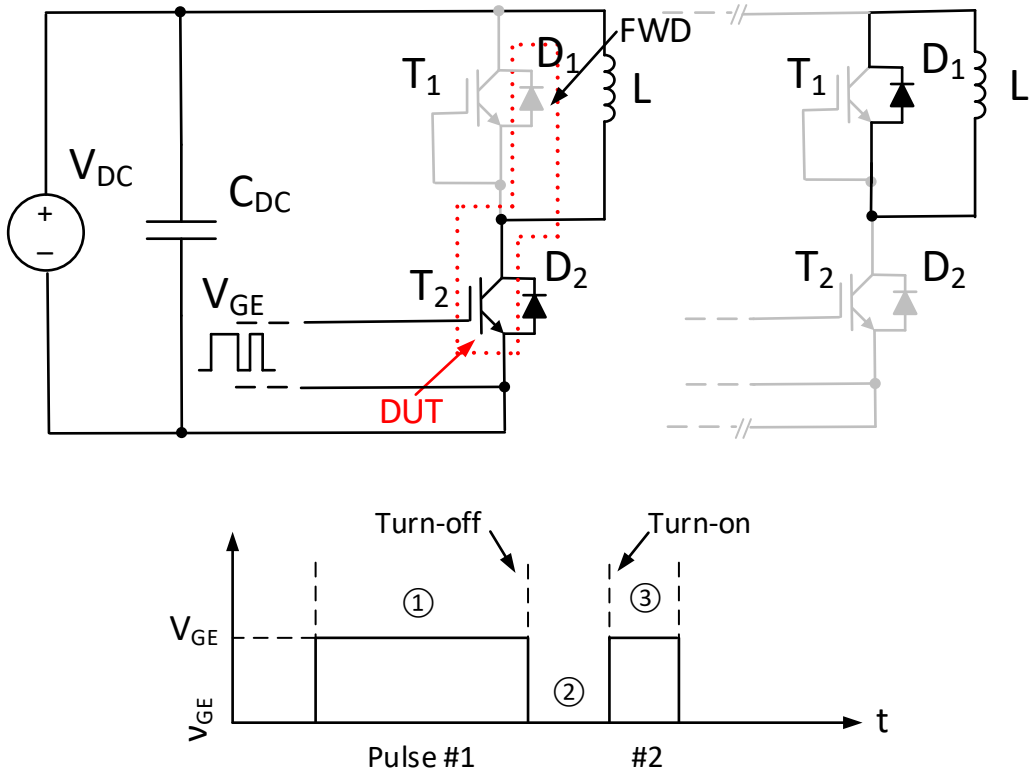

Figure 2 Double pulse test circuit (upper) and switch pulse waveform (lower), redraw from [35]

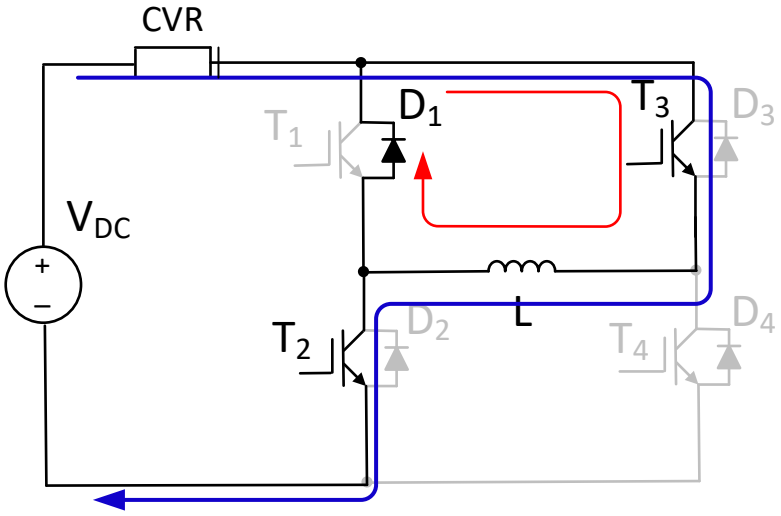

Figure 3 Double pulse tester with full bridge topology, redraw from [36]

1.3 Cooling System

1.3.1 Introductions of Types of Cooling System

Although the evaluation of semiconductors advances with the times, heat dissipation is still ineluctable. According to contents in the previous section, semiconductor heat loss is an inevitable fact in practice. The cooling system is constructed for heat dissipating purposes to reduce the semiconductor temperature; hence the lifetime and reliability of the whole system can be extended.

The types of cooling systems can be classified into passive cooling systems and active cooling systems. A passive cooling system is a cooling method that does not require an external power source, e.g., alloy heatsinks and natural cooling by air. The active cooling system stands for an external-powered cooling technique like liquid cooling pumps or electrical fans to accelerate the airflow around target devices.

Heatsinks normally are made of aluminum alloy and made with circular symmetrical fins in columns as a passive element for heat dissipation. The alloy constitution, volume, and the number of fins determine the thermal capacity of the heatsink [38]. Some of the typical configurations of heatsinks are shown in Figure 4. Benefited from the much larger thermal diffusivity of silicon than alumina ceramic implies a higher heat flux per unit concentration gradient, polycrystalline silicon package is recommended by the end of the 20^{th} century [39]. As mentioned in the previous chapter 1.2.1, GaN switches have the advantages of low switching loss and on-resistance which remarkably reduce the weight and volume requirement of alloy heatsinks rather than SiC MOSFETs and Si IGBTs [40].

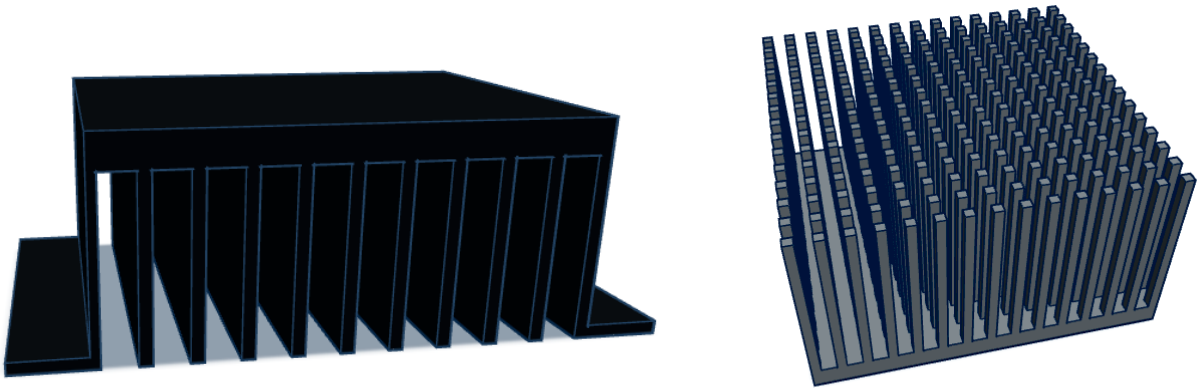

Figure 4 Examples of typical heatsinks designs

The model of heatsink application to a semiconductor is shown in Figure 5. Each layer of the contact surfaces from the semiconductor (labelled as heat source in the graph), the component mount surface, the thermal foil, and the heatsink surface [41]. As the alloy has a larger thermal capacity, it can absorb more heat energy from the source, then the temperature of components will be reduced.

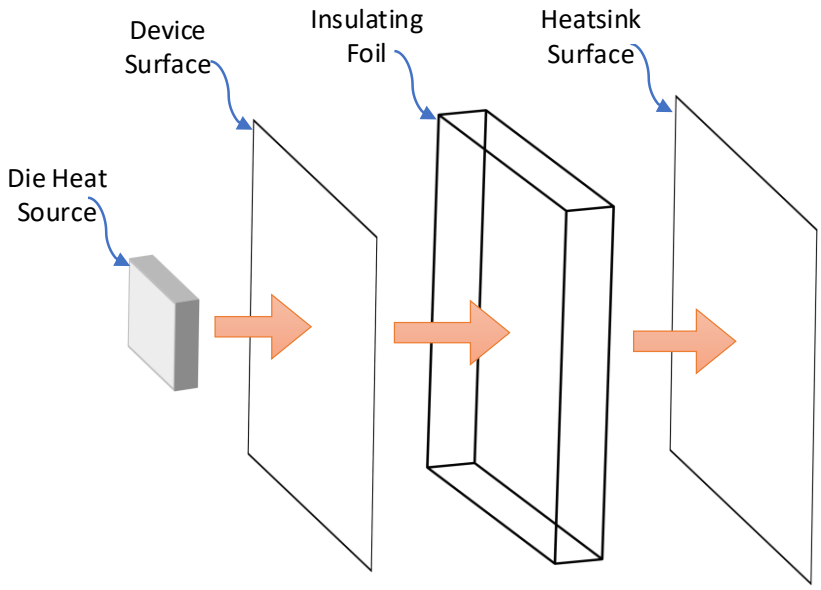

Figure 5 Layer models of application of heatsink to semiconductor

Liquid cooling system includes traditional coolant pumps for vehicles engine [42] and evaporative cooling systems for hydro-turbo generators [43], air cooling condenser for large-size electrical converters, and heatsink for power semiconductors and microprocessors [44]. Depending on the implementation of heat generator devices, the above-listed cooling method is chosen considerably for its own advantages and drawbacks.

Water and metal circulation are both effective materials as coolants. To improve the thermal capacity of the liquid, nanoparticles are added to the liquid. Since water has a much larger heat convection coefficient than air (over 200 times larger), and is convenient and low-cost, it became a popular choice in turbine generators and large electrical equipment like HVDC circuit breakers [45].

Evaporation technology owns the advantage of high heat exchange efficiency, and self-regulation of cooling ability and is widely used in electromagnetic separators [46], hydro generators, etc. The newly developed self-circulating evaporative cooling technology takes more benefits of high stability, high insulation, and lower consumption of coolant material. Besides that, in low-temperature environments, the evaporation cooling method is forced to be applied as a secondary cooling system for the air-cooling condenser [47]. Power dissipation of high-performance computing microprocessors used in machine learning significantly raises with the increase in the number of cores and system frequency. It brings a lot of challenges to the existing air-cooling technology. As the cooling demand grows, cooling technology evolves from passive air cooling to advanced air cooling and then to active liquid cooling technology.

1.3.2 Cooling System Design Methodology

The commercial computational fluid dynamics (CFD) software package from ANSYS Fluent is a popular method to analyze the thermal behavior of electrical and electronic applications, e.g., the thermal management of notebook computers [48], the diffuser of a micro wind turbine [49], and the heat path through each component of a SiC package [50]. Different steady-state conditions are applied to the passive and active cooling methods, then the output results are compared with the maximum allowable ambient temperature to determine the performance of the tested cooling method.

Finite Element Analysis (FEA), a newly developed algorithm, is implemented in air-cooled heatsink design [51]. However, the absence of airflow rate and pressure drop dominants the limitation in the optimization process. Simplified heat source by ignoring the layer of substrate and thermal coupling between them leads to lower computational capability. Genetic Algorithm (GA) with self-evolved machine-learning features and high accuracy of FEA together examine the different geometric configurations of heatsink to achieve the lowest device junction temperature in different conditions [52].

Another study presented a Hybrid Analytical Thermal Topology Optimization (HATTO) approach that maps external surfaces with inner heat transfer. After removing the weight from the base fin, the maximum heat rejection capacity is maintained and obtains better performance than the reduced-length fins when applying the same surrounding heat flow in simulation. The HATTO approach introduces a less sophisticated formation of heatsink design when reducing the length and height to minimize the weight and size of the heatsink. Obviously, the more complex geometric composition is, the higher thermal capacity it has. However, the cost of manufacturing

will also increase [53]. The simulation results show a tradeoff between cooling system performance and their cost in specific applications and conditions.

The above paragraphs listed different methodologies of the cooling system and their applications, and various designs. Fundamentally, the choice of cooling system depends on the heat dissipation specification. However, normal tests in physical conditions give unexpected results due to mutual temperature impact on components that are contiguous to each other. Simulation of the thermal model of the semiconductor and chosen cooling system can help with the cooling system design.

1.4 Real-Time Simulation

1.4.1 Offline Simulation and its Limitation

The simulation software is established by building mathematical equations of components' behavior and systems. This process requires solving large quantities of complex differentiations and integrations which may not be directly solved. Normally the mathematical expressions of the electrical components and systems are continuous equations in time domain, which are solvable numerical methods.

Off-line simulation is referred to ‘Simulation-In-the-Loop (SIL)’ as the completed system is built inside software programs, external signals cannot be input and interact with the models. While solving integrations by numerical methods, smaller time step produces a more accurate result. This requires a much smaller simulation time step rather than the dynamic of the system. Normally the simulation time step of off-line simulators is in a unit of microseconds. For a fast-dynamic system, although the overall shape is correct, the result will not be precise enough in detail compared to real experimental results [54].

Real-time simulation stands for that the actual time duration of the simulator to finalize this execution is equal to the simulation time that was set in the software program. This allows interaction between software programs and hardware signals at the correct instance [55].

1.4.2 Advantages of Real-Time Simulation

Hardware-In-the-Loop (HIL) simulation is a popular methodology to emulate power system networks, controllers, and complexity plants e.g. photovoltaic plants for smart grids. By building the mathematical module of the power system or circuit in the software, the output terminal generates the corresponding signal in low voltage or low current. Usually, power

electronics like converters, controllers, or a section of the whole power system are implemented as the hardware subsystem. The core conceptualization of HIL is generating simulation results and communication hardware physical signals simultaneously. This allows the simulation in real-time and provides more accurate results compared to normal offline imitation [56]-[57].

Figure 6 illustrates the configuration of common PHIL including the Real-Time Simulation Software (RSCAD) simulator [58]. The typical execution time step of RSCAD simulation is around $25\mu s$ to $50\mu s$. The embedded analogue-to-digital converter (ADC) and digital-to-analog converter (DAC) scale and transmit the signal from modules in software and hardware device under test (DUT). The high-power section is established in software by using built-in modules in the program which enables easy modifications of any settings of the test environment conditions. Additional amplifiers are required to restore the signal to its original size e.g. hundreds or thousands of watts in power or tens of thousands of volts of voltage to recover the test qualification for DUT.

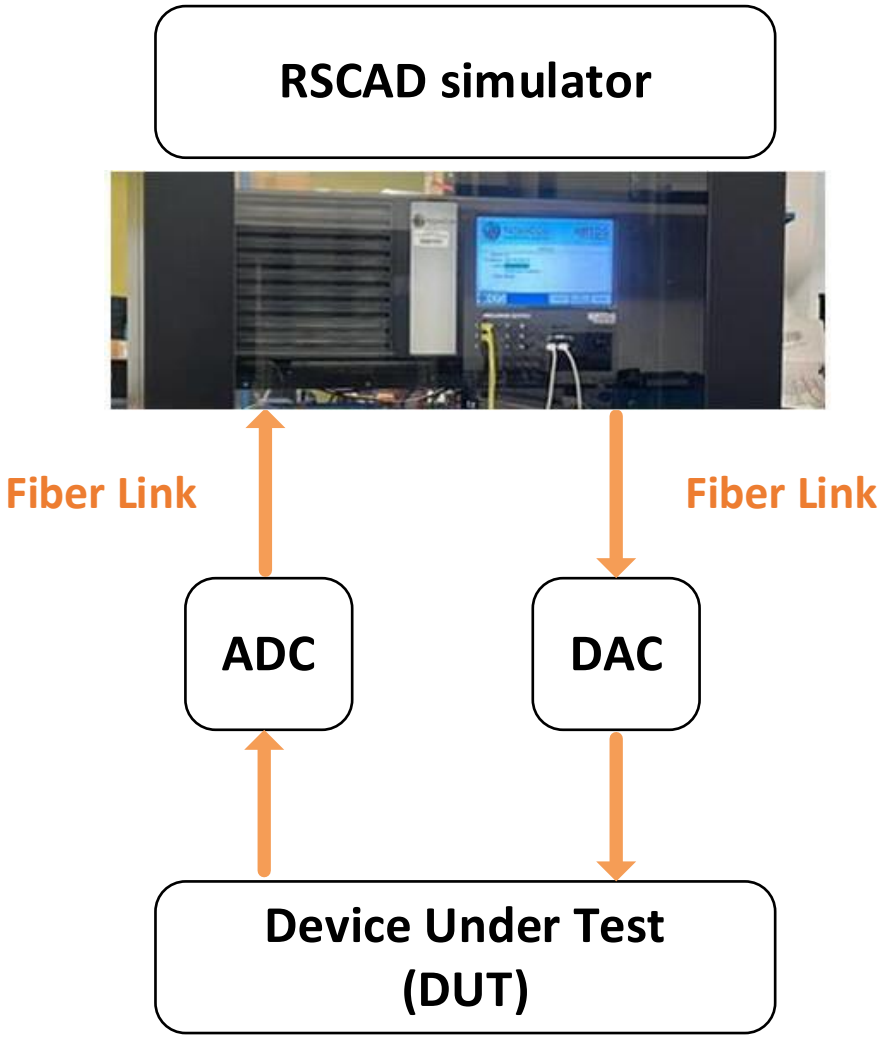

Figure 6 RSCAD simulator with typical implementation

This methodology allows separation between high-power apparatus and the DUTs to enhance the safety and stability of simulation processes. Any error that occurs in the DUT like overcurrent or overheating has a probability to damage the rest of the circuit in traditional full circuit experiments. In HIL simulation, the measured data will be scaled and converted to digital signals and then send to RSCAD simulation. Supplementary maximum and minimum values can be set in the program to forbid extreme values that influence the main power circuit.

1.5 Motivations of the Thesis

As mentioned in the background sections, the semiconductor power loss is critical in the determination of its efficiency, fidelity, and lifetime and strongly depends on its temperature. Thus, the cooling system is necessary for the overall power electronic designs. Millions of cooling systems are available in the market to meet various heat power dissipation specifications and further physical tests are needed before operationalization.

Inspired by the popular methodology of Power Hardware In-the-Loop (PHIL), a semi-physical platform to evaluate cooling system performance in real time is concretely proposed in this Thesis. The model of the semiconductor is built inside a real-time simulator, then estimation of junction temperature and instantaneous power loss of semiconductors. After preliminary measurements of the semiconductor conduction and switching characteristics are done. These characteristics are modified to build the mathematical approaches to represent the semiconductor loss models. Finally, the thermal network of the cooling system is assembled by the given information in the datasheet. By connecting the software and hardware, the overall THIL system is completed and generates real-time results for the semiconductor power loss and dynamic and steady-state temperature.

1.6 Thesis Objective

The objective is to design and implement a real time a semi-physical evaluation platform of cooling system for dissipating semiconductors in power circuits. The sub-objectives are shown below:

- Building a correct semiconductor model corresponding to current, voltage, and temperature in software. This requires comparing simulation result with the actual physical diode to verify if this IVT model is accurate or not.
- Creating a thermal RC circuit for the power semiconductor applied with the chosen cooling method which is a heatsink in this study. This heatsink thermal model is confirmed by comparing the simulation heatsink temperature with the experimental measured temperature.
- There should be a power interface device between the software program and the cooling system (DUT) to generate same power output as the software simulated. The device should have a faster dynamic than the whole T-HIL system.
- The estimated junction temperature should be maintained below the maximum temperature limitation. This provides sufficient evidence that the choice of cooling system is suitable.

1.7 Organization of the Thesis

This thesis is organized into five chapters. A brief introduction of the chapters is as follows:

Chapter 1: Introduction – This first chapter classifies the background information related to this thesis, literature review, and motivation of this research. Because of the ineluctable loss of semiconductors, the importance of cooling systems is highlighted. To maintain the stability, accuracy, and fidelity of the semiconductors, different cooling methods are chosen depending on the heat dissipation demand and cost. The contribution of the thesis is also included in this chapter.

Chapter 2: Operation Principle – This chapter details proposed a semi-physical THIL simulation to evaluate the cooling system as a new convenient and low-cost procedure. The configurations of both software and hardware sections are shown in block diagrams. The comprehensive working principle is clarified from step to step and the overall system is completed by transmitting simulated and measured signals between the two sections respectively.

Chapter 3: Developments of critical components in THIL – This chapter discusses all the important components in the THIL system, including the development and simplification of the thermal network, analysis of the electrical resistance behaviour of the aluminium heater with respect to temperature, circuit architecture and control strategy of switched-mode power amplifier, the establishment of thermal loss model based on validation of diode voltage-current-temperature (VIT) characteristics and the communication interface accuracy. Each element is explained for its configuration and operating principle.

Chapter 4: Experiments and Results – The physical experimental test bench is set up in the laboratory. The open-loop test that disconnects the temperature feedback is evaluated first to verify the thermal circuit and software semiconductor VIT models. After the approval of the open-loop

result, the closed-loop test is completed by connecting the feedback terminal to the real-time simulator. The final result of junction temperature estimation is demonstrated in this chapter for different power dissipation.

Chapter 5: Conclusion and Future Work – This chapter summarized the core contents of the whole thesis from background research and system architecture to the final experimental result. Future extensions that applied this THIL simulation with multi-semiconductor and high-frequency converters are discussed.

1.8 Research Contributions

This thesis proposed a Thermal Hardware-In-the-loop semi-physical method to evaluate cooling system performance which is lower in cost and higher in efficiency compared to traditional experimental tests.

The main contributions of this research are concluded and listed below:

- A comprehensive background information study about semiconductor power loss, cooling system development, and evaluation topology. The importance of the cooling system in power electronics is emphasized and more ways to test its functionality are created continuously.
- The proposed Thermal Hardware-In-the-Loop semi-physical simulation methodology provides a high-efficiency and low-cost way to evaluate the cooling system. Additionally, the real-time power dissipation and junction temperature are together estimated.
- The switched-mode power converter is constructed to generate corresponding power output relative to the given reference signal. The control strategy and circuit topology are discussed.
- The thermal network is developed and simplified for software models. The open loop results validate the heatsink-to-case junction resistor-capacitor (RC) circuit of the thermal network. Hence, the junction temperature is assessed by information provided by the datasheet of junction-to-case connection.
- This contribution leads to the conference paper:

  C. N. M. Ho, **Y. Fang**, Y. Xu, and I. Jayawardana, "Thermal-HIL Real-Time Testing Platform for Evaluating Cooling Systems of Power Rectifiers," 2021 IEEE Energy Conversion Congress and Exposition (ECCE), 2021, pp. 5729-5734 [59]

Chapter 2 System Overview

A novel Thermal-HIL real-time simulation system for evaluating physical cooling systems for dissipating power semiconductor losses is proposed in this chapter. The overall system shows in Figure 7, which aims to evaluate the thermal dynamics of a cooling system by using a physical DUT but with a simulated circuit and a power semiconductor model in an RTS. The approach can effectively reduce the design cost and time for designing cooling systems for high-power rectifiers since there is no real high-power circuit in the testing platform. It also can be used as a burn-in system for testing the reliability of a cooling system. This thesis provides the conceptual idea of the T-HIL system design and elaborates on the operating principle of the proposed T-HIL system.

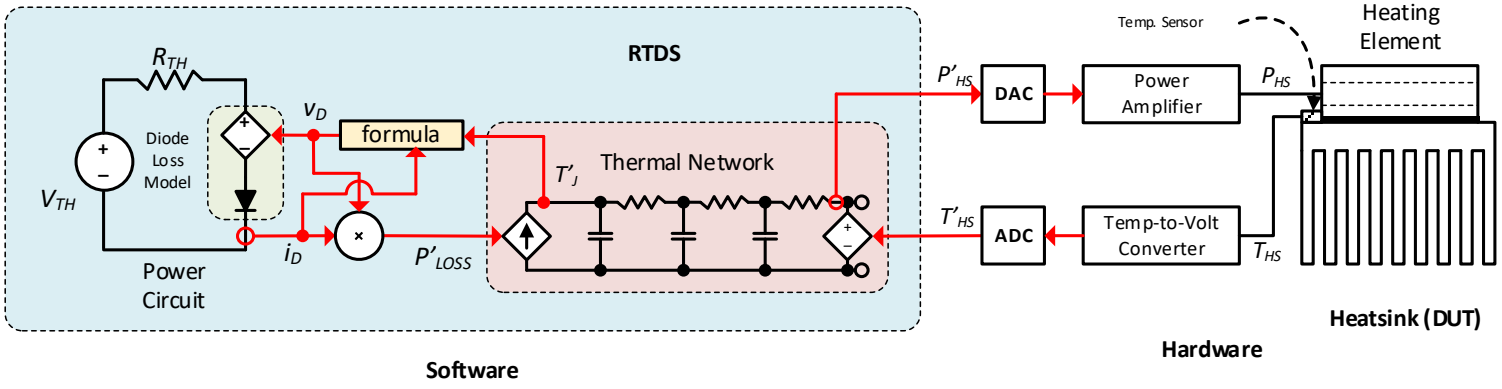

Figure 7 Overall system block diagram of Thermal-HIL system.

2.1 Software Section

The software section consists of the real-time software simulation application (RSCAD), Real-time digital Simulator (RTS), Analogue-to-Digital (ADC) interference, and Digital-to-Analogue (DAC) interference, ADC and DAC are required as a communication interface between high-performance computer RTS and external hardware system.

A diode conduction circuit is built in software and runs in RTS real-time to emulate semiconductor power loss. The block diagram in Figure 7 shows three main parts in software: the diode conduction circuit, the diode characteristic interpolation, and the thermal RC circuit. The power circuit simulates the target diode where the real semiconductor is modified as an ideal diode cascade with a voltage-controlled voltage source (VCVS) shown in Figure 8. The voltage source represents the diode forward voltage drop depending on the operating current and temperature. A voltage-current-temperature relationship formula interpolation was built to determine the operating voltage by sensing the current through the diode and estimating its junction temperature.

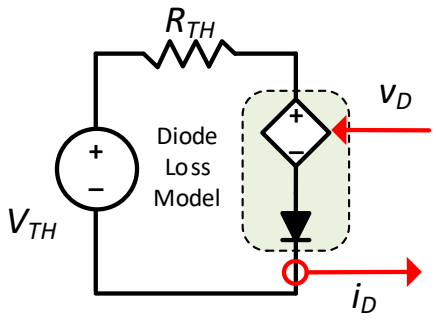

Figure 8 Diode conduction circuit in RSCAD software program

The load line expression of the conduction circuit is shown in equation (1):

$$I_D = -\frac{1}{R_{TH}} V_D + \frac{V_{TH}}{R_{TH}} \qquad (1)$$

$$I_D = f(V_D) = \begin{cases} 0, & V_D < V_{th} \\ \frac{(V_D - V_{th})}{R_D}, & V_D \geq V_{th} \end{cases}, \qquad (2)$$

Same as labelled in Figure 8, V_D and I_D is the forward voltage and current of the diode, V_{TH} is the constant voltage source, and R_{TH} is the series conduction resistance. Shown in Figure 9, this load line (blue) has an intersection with the diode IV characteristic (yellow) shown in equation (2) at this specific temperature, which is the operating point of the diode. The blue dots illustrate how the measured diode voltage and current approach to the intersection in simulation from the instance the diode begins to conduct. From the simulation software, it takes about 0.25 seconds to reach the intersection, and this is acceptable for the T-HIL system.

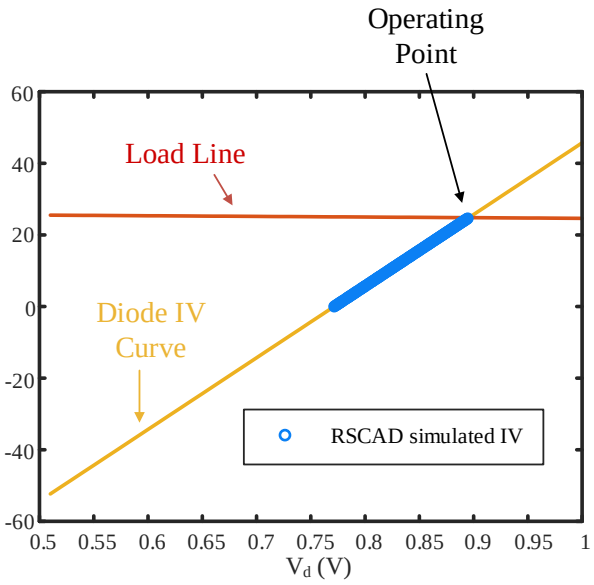

Figure 9 Diode IV characteristic at transient

Surprisingly, the diode forward characteristic shows a significant difference between the datasheet and the experimental result. The linear assumption of the diode is supposed to modify the forward current and voltage (IV) characteristics. Once the forward voltage is determined from the formula interpolation, the power dissipation is calculated and sent to the thermal RC circuit shown in Figure 10. The thermal resistance and capacitance are modified by fitting the temperature-time diagram and its transfer function. By receiving the measured temperature signal from ADC, the junction temperature of the diode can be estimated in the thermal circuit and sent back to the LUT to allocate the new operating point of the diode.

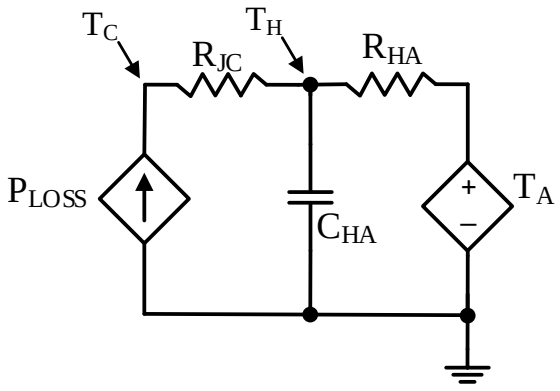

Figure 10 Thermal RC network

2.2 Hardware Section

The hardware section consists of the physical setup of the cooling system that is the device under test (DUT), a heating element that is used to emulate heat energy dissipation of real semiconductors, a power amplifier controls the power output to the heating element which is generated by diode conduction model in software. As shown in Figure 11, the heater is placed on a heatsink or within other active cooling systems, then the surface temperature is monitored by an analog thermal coupler and is scaled and sent back to RTS. The diode power dissipation generated by the software is also transmitted from the DAC interference to a power amplifier (PA) which controls the output power to a constant heater.

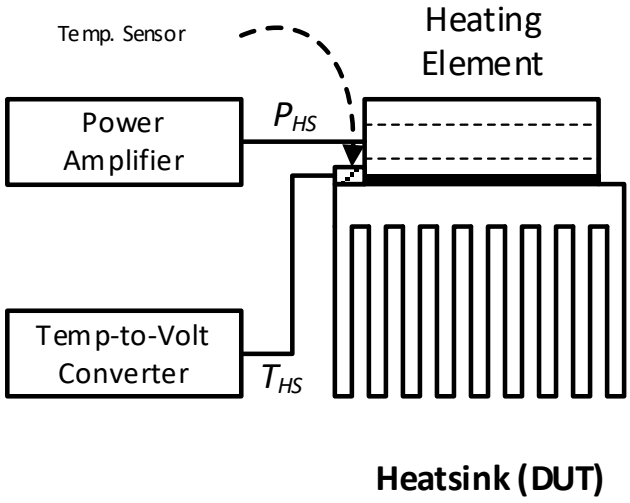

Figure 11 Hardware section setup

A simplified block diagram is shown in Figure 12 to indicate the signal transmission between the software and hardware interface. The whole software simulation program is simplified as a Norton equivalent circuit that generates the power reference signal and is sent to the hardware circuit. The hardware section is also modified as a Norton circuit to output the heatsink temperature and sends it back to the program.

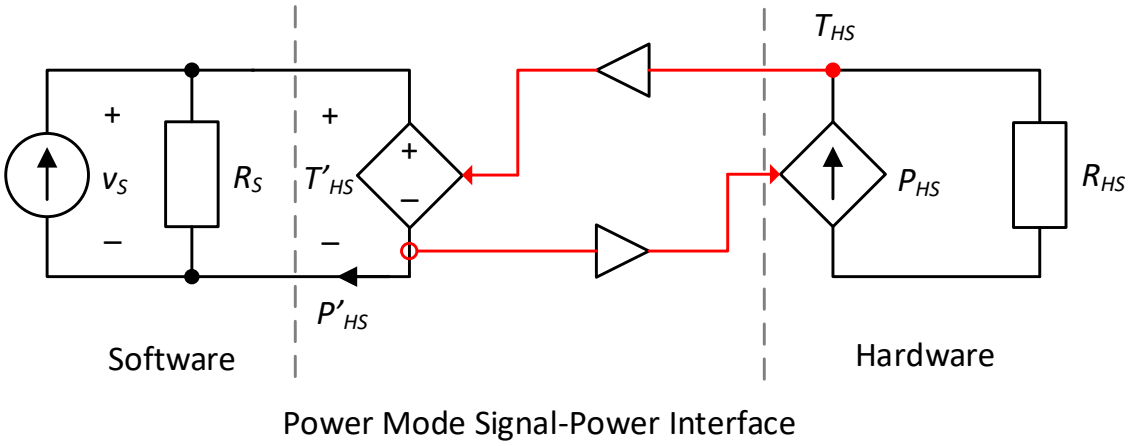

Figure 12 Simplified overall system block diagram

2.3 Chapter Summary

This chapter introduced the overall system architecture and the working principle of the T-HIL cooling system evaluation method. The function of each block in software and hardware is present while the transmission of a signal between software simulation and hardware measurement is emphasized to form the closed loop.

Chapter 3 Development of critical components in THIL

3.1 Diode behavior validation

The diode behavior information is usually given in the component datasheet. However, in real experiments, the forward voltage and current of the diode have a significant difference from the given data. The comparison is shown in Figure 13. To obtain an accurate diode VIT relationship interpolation, a simple diode conduction circuit shown in Figure 14 is built with a current source, a heater is used to heat the diode to a specific temperature, and a temperature sensor monitors the instantaneous temperature, a voltage probe, and a current probe connecting to the oscilloscope to measure the IV data. The forward voltage of the diode is measured at $25°C$ and $100°C$ by the given current source at 5A, 10A, and 20A.

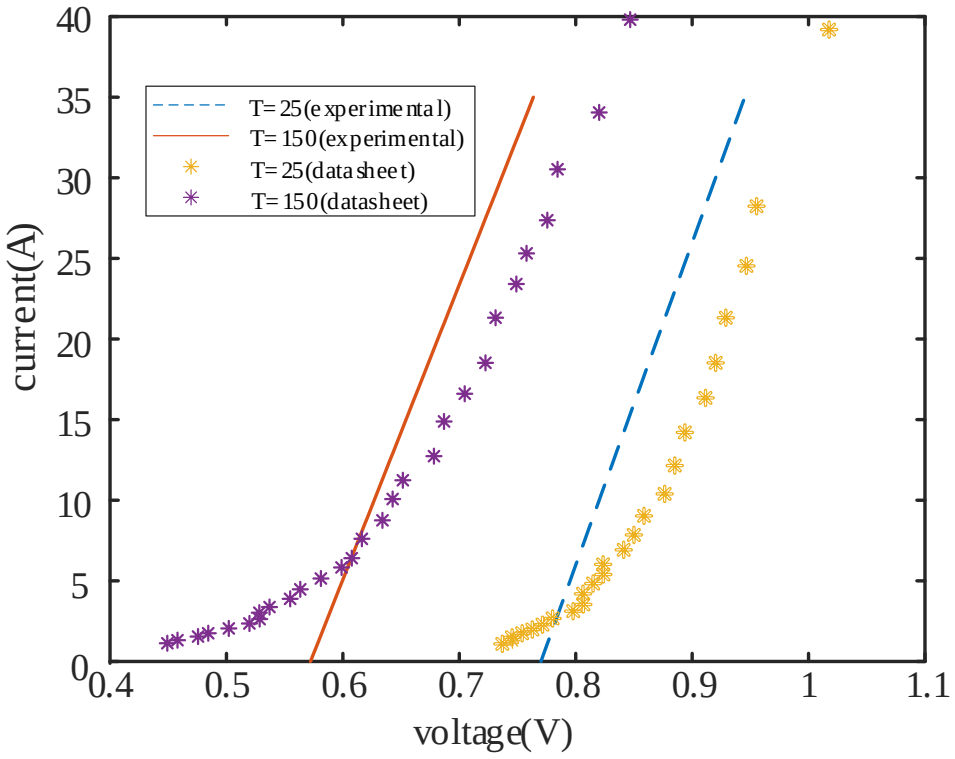

Figure 13 Comparison diode IV behaviour from datasheet and physical test at 25°C and 150°C

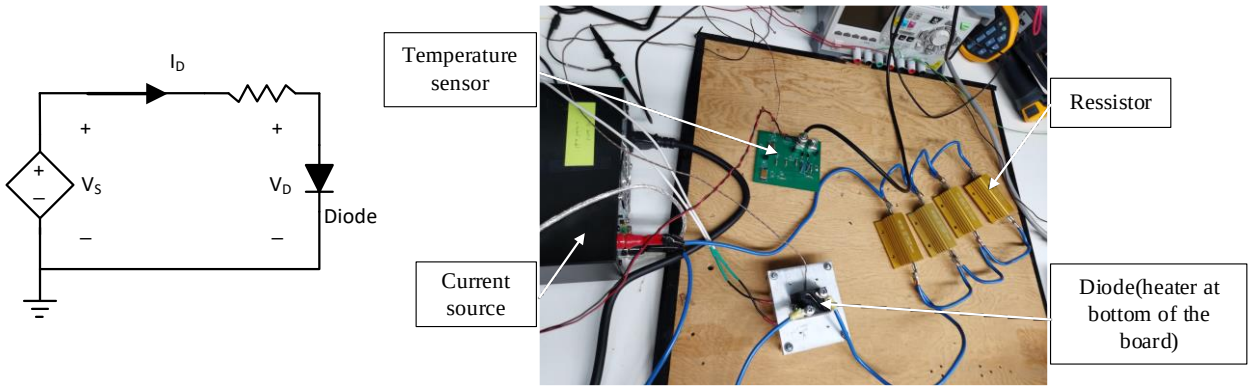

(a) (b)

Figure 14 Diode behaviour test circuit (a)schematic circuit (b) physical set-up

The diode threshold voltage (V_{th}) and the diode resistance (R_D) are initially obtained by a linear assumption of diode IV behavior based on the following equation (2),

$$I_D = f(V_D) = \begin{cases} 0, & V_D < V_{th} \\ \frac{(V_D - V_{th})}{R_D}, & V_D \geq V_{th} \end{cases}, \qquad (2)$$

where I_D and V_D are diode forward current and voltage, respectively. A 3-dimensional VIT (voltage, current, and temperature) relationship is found according to the diode's current-voltage (IV) data at 25°C and 150°C in experimental result. Based on measurements of diode forward voltage and current at the same temperature, R_D and V_{th} can be calculated by equation (2). Then the diode conducts for different temperatures and these two characteristic parameters are plotted in Figure 15. From the plot, the linear relationship between R_D and V_{th} with respect to temperature is found. The diode IV relationship at different temperatures is shown in Figure 16 as a visualization of the linear assumption.

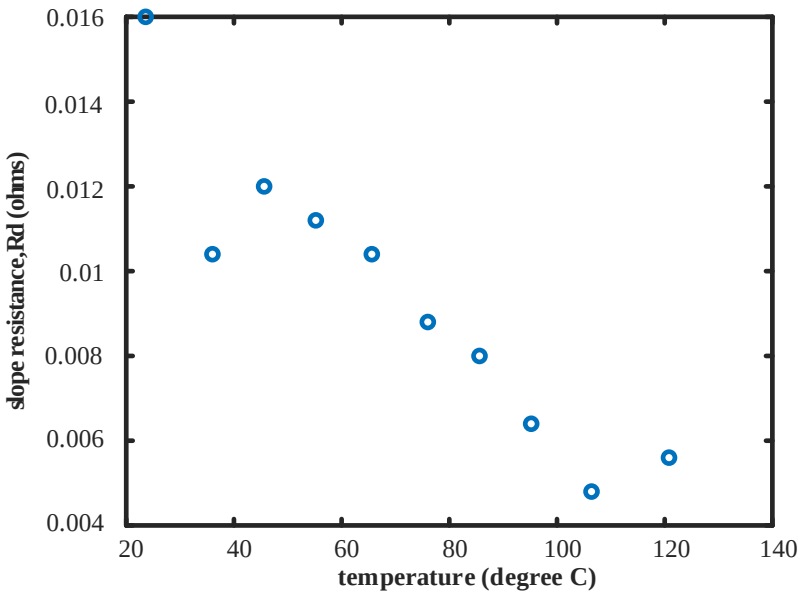

(a)

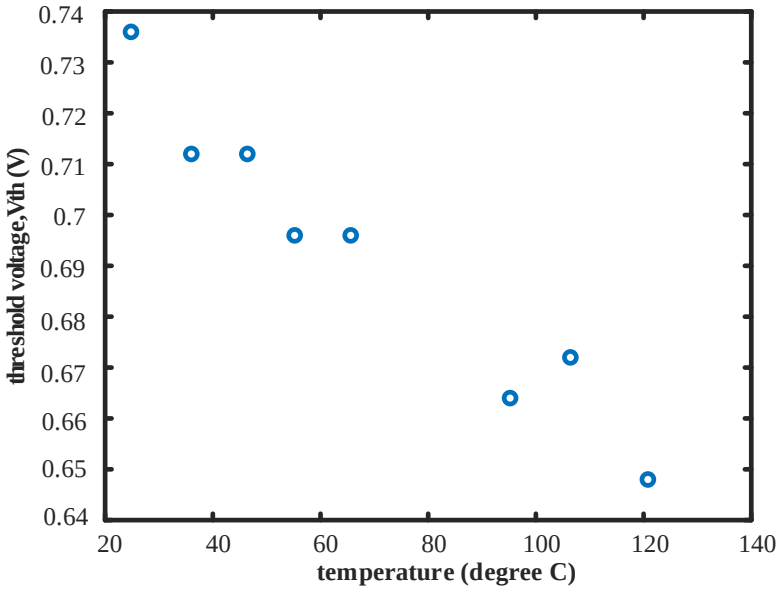

(b)

Figure 15 (a) Slope resistance (Rd) and (b) threshold voltage(Vth) are plot with respect to temperature

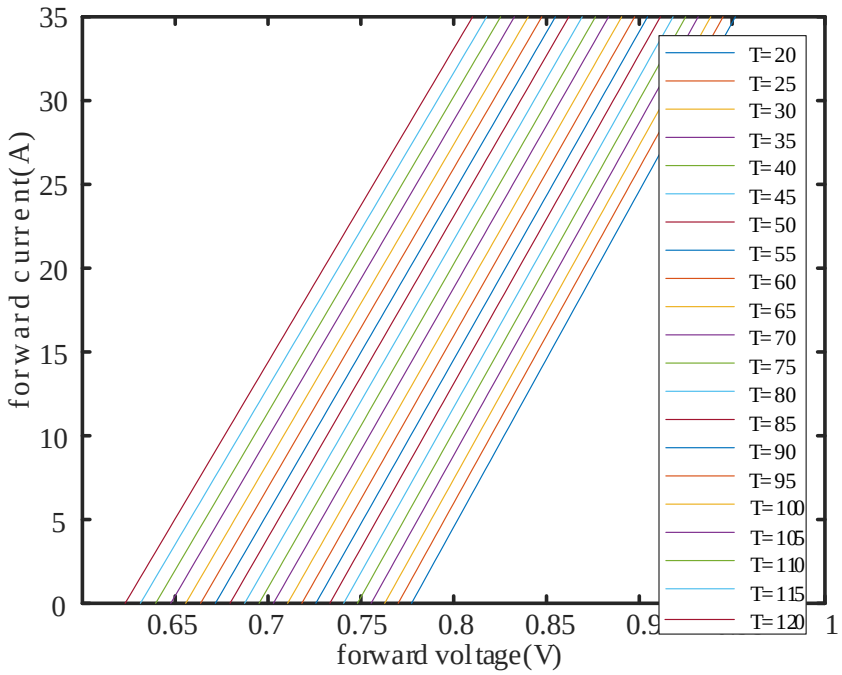

Figure 16 Diode voltage and current relationship at a temperature between 20°C to 120°C

In the software diode VIT interpolation module, the slope, and interception of the IV linear relationship are first calculated by junction temperature. The instantaneous junction temperature is estimated by physical thermal coupler measured data as heatsink temperature. Hence instantaneous forward voltage is worked out by measured current in the software diode conduction circuit and newly calculated linear slope and an interception at this operating temperature.

3.2 Development of loss-thermal circuit mode

The loss-thermal model is built to determine the semiconductor's instantaneous forward voltage at operating temperature and calculate its power loss. The algorithm of the thermal-loss model is shown in Figure 17, forward voltage is calculated from measured current and estimated temperature. Based on that, instantaneous power loss is estimated by forwarding voltage multiplies operating current and sent to both software thermal model in RTS and through digital-to-analog (DAC) interface to external power amplifier as target power output. The heatsink temperature data are collected by a temperature sensor and then through an analog-to-digital (ADC) to RSCAD software and represented by the voltage-controlled voltage source in the diode conduction circuit to modify instantaneous forward voltage drop. Instantaneous power is modified as a voltage source in the thermal circuit, so the junction temperature is estimated and simulated in software. Finally, the updated temperature is transmitted back to the interpolation for the diode to locate the operating point for the next iteration.

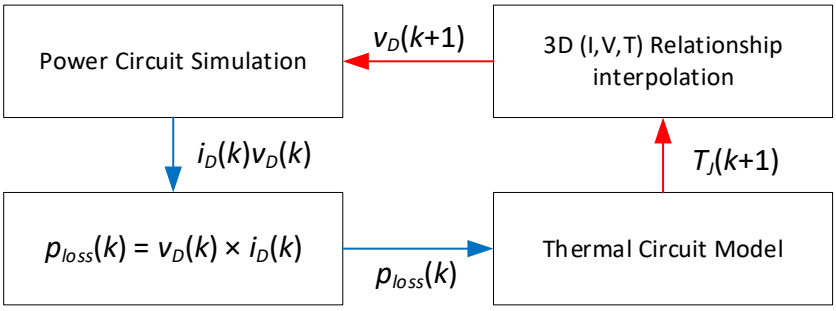

Figure 17 Thermal-loss interpolation algorithm

3.3 Thermal Network Development

Generally, there are three different methods to evaluate the thermal performance of a cooling system: (1) the analytic approach, (2) the numerical approach, and (3) the equivalent thermal circuit approach [60]. The first two approaches require a detailed component structure and material information to make complicated modeling with a long simulation time. The last approach is modeled by connecting a series of resistors and capacitors in two different configurations as shown in Figure 18.

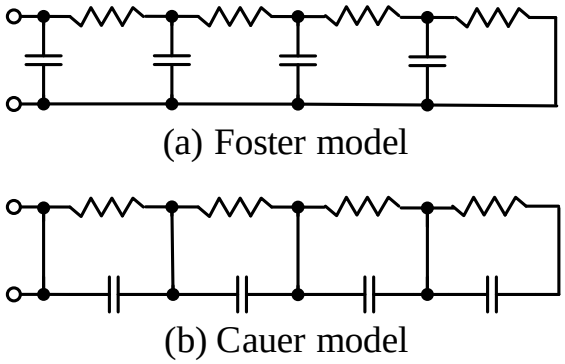

Figure 18 Equivalent circuits of the thermal circuit, (a) Foster model and (b) Cauer model

Both models describe the thermal transfer at critical nodes of the system, i.e. junction, case, heatsink, and ambient. In comparison, the Cauer model provides a more practical description of the thermal model as the capacitor needs time to be charged up so heat takes time to reach the ambient node in this circuit. For Foster modeling, the series resistors determine the voltage at the instant while the heat power dissipation is applied. However, the Foster model is easier to approach by fitting measurement or simulation curves to semiconductor temperature with respect to time[61].

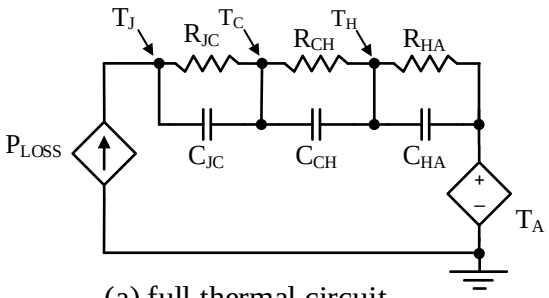

(a) full thermal circuit

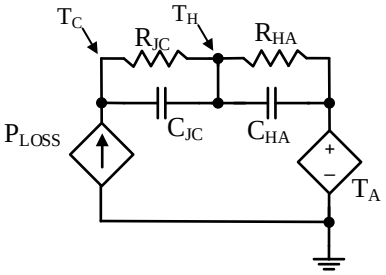

(b) simplified thermal circuit

Figure 19 Simplification of the thermal RC network

Therefore, the Cauer model is used in all critical junctions. Firstly, the parameters of junction-to-case section are extracted from the datasheet. Secondly, after applying high-quality thermal grease between diode and heatsink, the case RC section can be neglected. The circuit is further simplified in Figure 19(b). The transfer function in the time domain is given in equation (3) of heatsink temperature ($T_{Heatsink}$) respect to time. The heatsink-to-ambient thermal resistance and capacitance are calculated by fitting the hardware experimental data to the expression.

$$T_{Heatsink} = P_{loss} \times R_{HA} \times \left(1 - e^{-\frac{t}{R_{HA} \cdot C_{HA}}}\right) + T_A \qquad (3)$$

3.4 Heating element electrical resistance behavior

The aluminum heating element is a self-regulating heater and is designed to provide a wide range of power output. In practical tests, the electrical resistance of the heating element varies with

temperature change. By curve fitting the physical experimental data of heater electrical resistance and operating temperature in MATLAB, a cubic relationship was found. The experimental data compared with cubic relationship expression is shown in Figure 20, the resistance reduced to half of its value at room temperature while the heater temperature rise to 99.4°C.

As a result of the non-constant electrical resistance of the heating element, a controlled power amplifier is necessary for the overall system to ensure the heater will output target power whatever the temperature is.

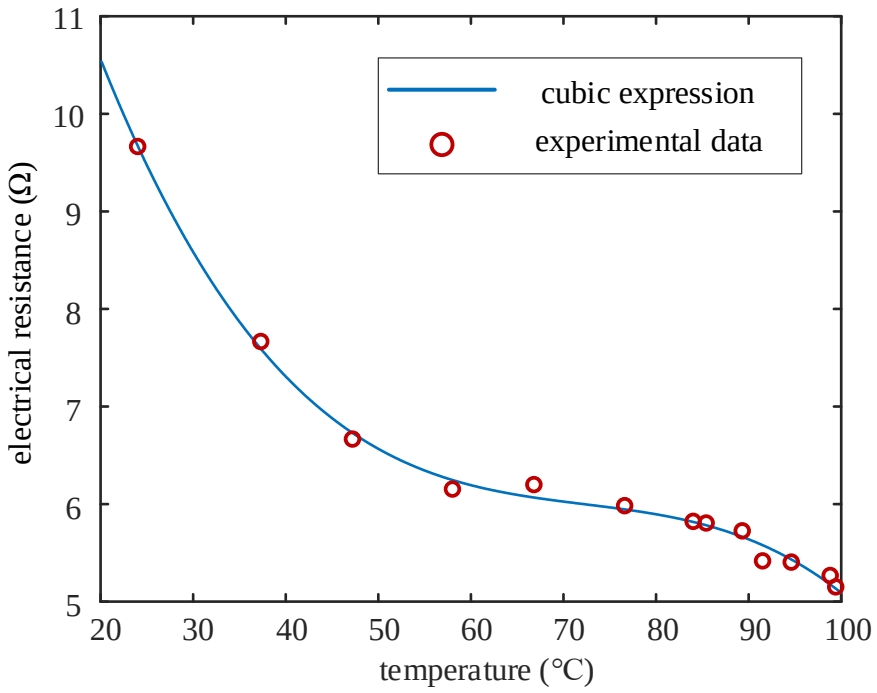

Figure 20 Curve fitting relationship from Experiment Data for Electrical Resistance of Aluminium Heater with Respect to Temperature

3.5 Development of a switched-mode power amplifier

3.5.1 System Overview

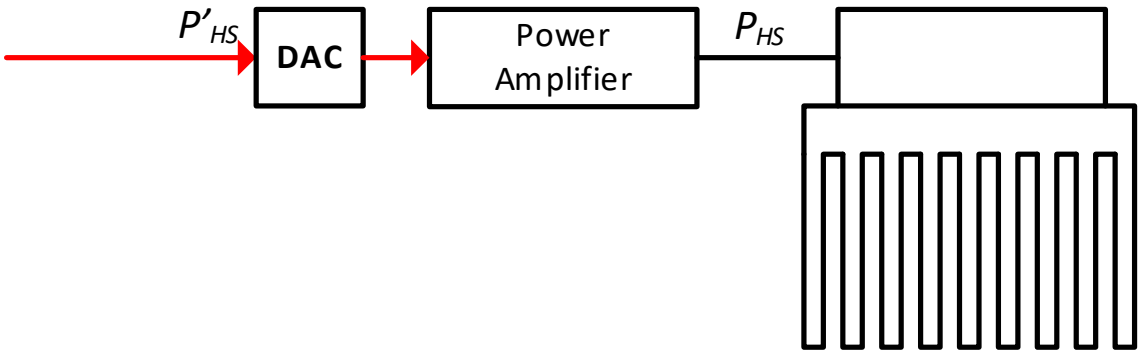

Figure 21 Power amplifier with input and output interface

The power amplifier is a critical component in the HIL system. The software program runs the real-time simulation and sent a scaled low-voltage signal to external terminal. This allows manipulation of the simulation signal and interaction with the hardware circuit. As shown in Figure 21, The power amplifier is used to receive the signal from a digital-to-analog (DAC) communication chip and rescale the signal to the actual value, then output the original value in the simulation. In this study, the PA receives a power reference signal that represents the diode instantaneous power loss, then the microprocessor adjusts the controller to generate corresponding output power. The output terminal of PA is connected to heat, thus producing the same heat dissipation as the simulated diode. The PA and heater together represent semiconductor instantaneous power loss and are applied to a heatsink which is the device under test (DUT).

3.5.2 Topology

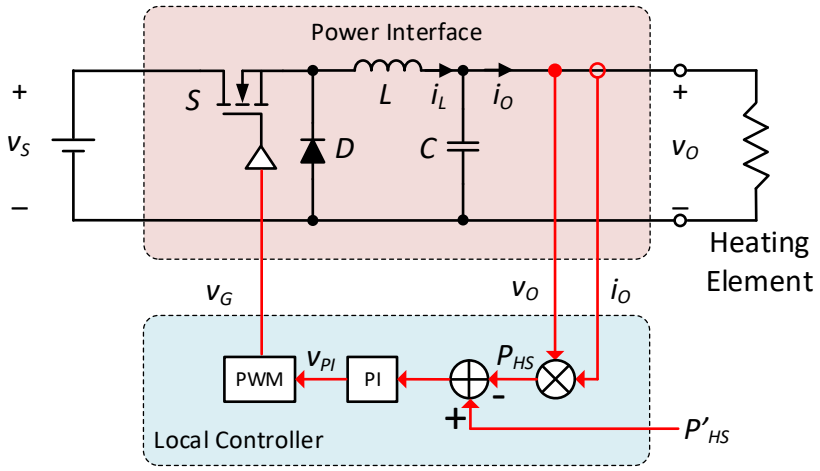

Figure 22 Power Amplifier System Structure

The power amplifier is implemented by a buck-based switched-mode amplifier to generate corresponding power output to the heating element whose individual system is shown in Figure 22. The output voltage and current are sensed, scaled, and sent to the local DSP controller then compared to the power reference. Based on the power loss range of the diode at all temperatures, the output voltage domain of the PA is up to 35 Watts. Additionally, with the same level of environmental noise, the low-voltage signal is affected more due to a smaller signal-to-noise ratio (SNR). The output voltage range is finally decided in the range from 10V to 20V and the input voltage o increases from 25V to 40V respectively. The DSP receives the power reference from RSCAD and calculates the corresponding duty cycle produce the targeted output power. The steady-state equations of buck converter are shown as follows:

$$\Delta I = \frac{V_S V_O}{(V_O - V_S) L f_s} \qquad (4)$$

$$\Delta V_o = \frac{I_O V_O}{(V_O - V_S) C f_s} \qquad (5)$$

ΔI and ΔV_o are output current and voltage ripples shown in Figure 23 of the output waveform diagrams. V_S is the source voltage, V_O is the output voltage, L and C are the passive components inductance and capacitance in Figure 22 and calculated by equations (4) and (5), and f_s is the converter switching frequency.

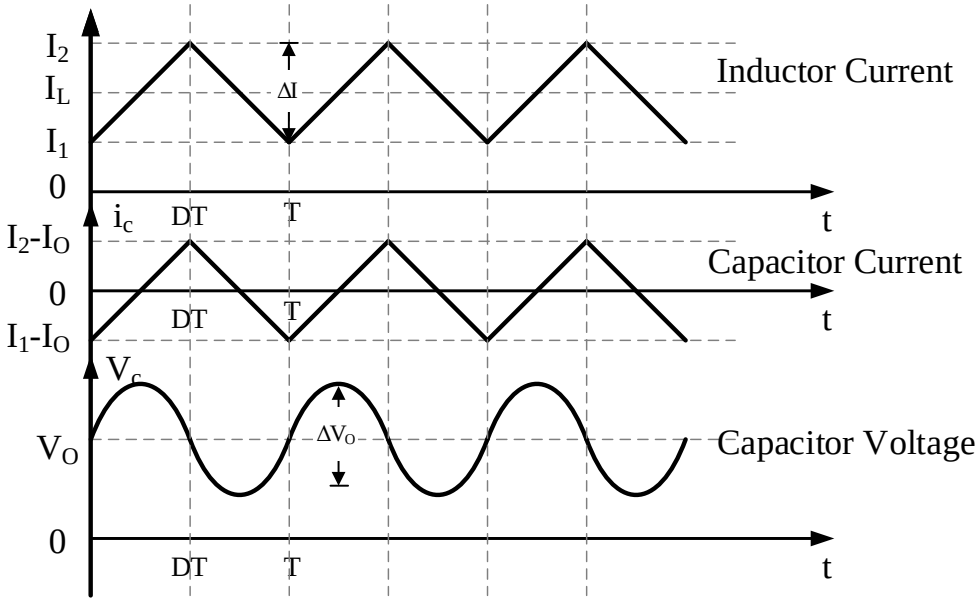

Figure 23 Buck converter output variable waveforms

Taking the output power of 15W as an example, the parameters are shown in Table 2.

Table 2 POWER AMPLIFIER PARAMETERS

Parameter	Value	Parameter	Value
Input Voltage	30 V	Output Voltage	11.4 V
K_P	0.03	K_I	100
L	1 mH	C	4.7 uF
R_H	5.3 Ω (high temperature) to 10.5 Ω (low temperature)		

3.5.3 Control system design

The DSP receives the power reference signal and restores it to its original value, then compares it with the measured voltage and current at the output terminal. The measured output power is subtracted from the power reference and the result is the error signal then is sent to a PI controller. The output of PI controller is compared with a triangular wave and the corresponding PWM signal is generated to the gate of the power semiconductor switch. The output voltage is controlled by adjusting the duty ratio of the switch so output power is further controlled.

The power amplifier is a closed loop controlled by local DSP. In order to determine the closed-loop system bandwidth, small signal modeling is applied.

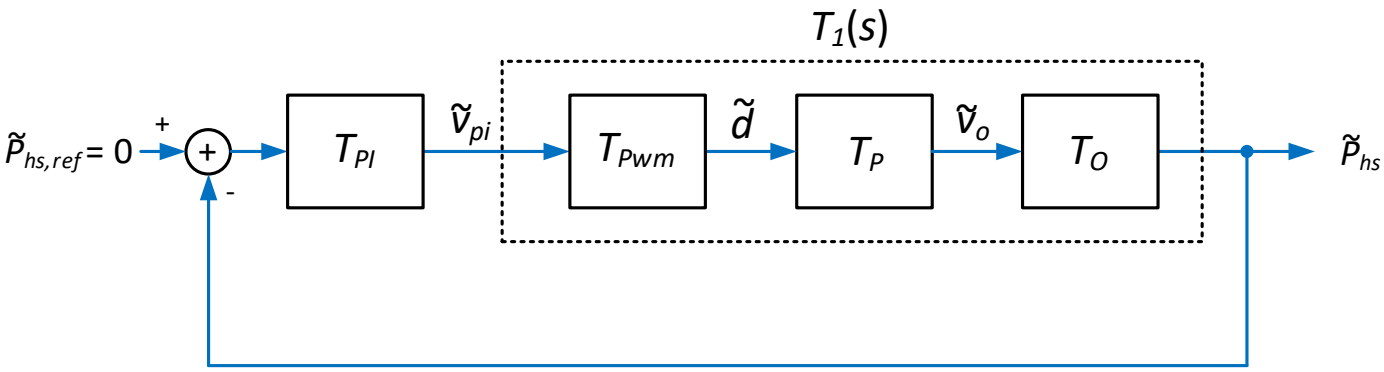

Figure 24 Small signal diagram of power amplifier

The overall small signal system of the power amplifier is illustrated in Figure 24 and expressions of each stage are shown in the following paragraph.

A. Transfer function of PI controller:

$$T_{PI} = \frac{K_P s + K_I}{s} \qquad (6)$$

B. Relationship between PI controller output signal and duty ratios:

$$T_{pwm}(s) = \frac{\tilde{d}}{\tilde{v}_{pi}} = \frac{1}{\hat{V}_r} \tag{7}$$

where d is the duty ratio, $v_{pi}(t)$ is the input signal of the modulator, $\hat{V}_r$ is the peak value of the carrier waveform as shown in Figure 25,

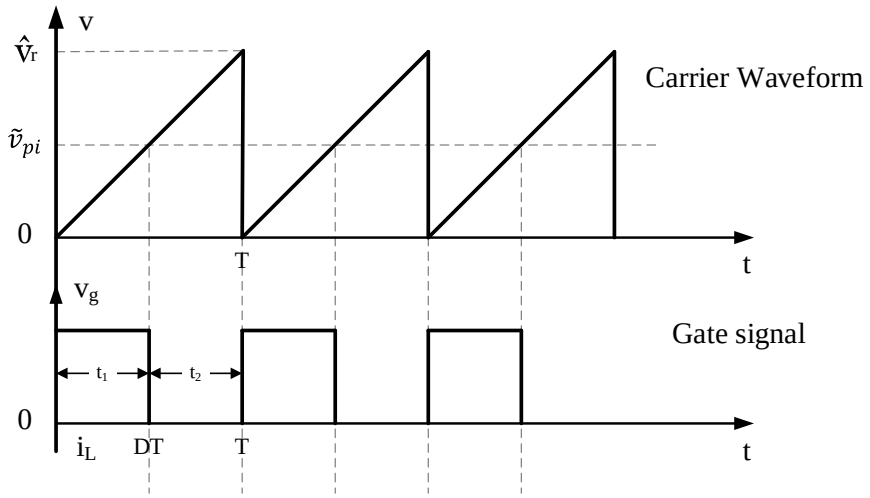

Figure 25 Carrier waveform and gate signal of buck converters

C. Relationship between duty ratios and output voltage:

$$T_P(s) = \frac{\tilde{v}_o}{\tilde{d}} = \left(\frac{V_S}{LC}\right) \frac{1}{s^2 + \left(\frac{1}{R_H C}\right)s + \frac{1}{LC}} \tag{8}$$

where L and C are the inductance and capacitance of the converter circuit shown in Figure 22, R_H is heat element resistance, and P_{HS} is output power to a heating element. By apply state space equation to this circuit, the transfer function can be solved.

D. Relationship between voltage and output power:

$$T_O(s) = \frac{\tilde{p}_{hs}}{\tilde{v}_o} = \frac{2V_O}{R_H} \tag{9}$$

So, the transfer function of the power plant (T_1) is:

$$T_1(s) = \left(\frac{2V_O V_S}{\hat{V}_r LCR_H}\right) \frac{1}{s^2 + \left(\frac{1}{R_H C}\right)s + \frac{1}{LC}} \qquad (10)$$

The electrical resistance of heater R_H is involved in both equations (9) and (10) and it varies with different temperatures.

The open loop system bode plot is shown in Figure 26 only for power plant T_1 and in Figure 27 for power plant with PI controller stage .After applying the PI controller as compensation, the phase margin of the open loop design is improved from 9.89° to 58° at low temperature and from 13.3° to 66.1° at high temperature. The phase margin is increased by about 45° which can provide sufficient compensation to maintain the system stability.

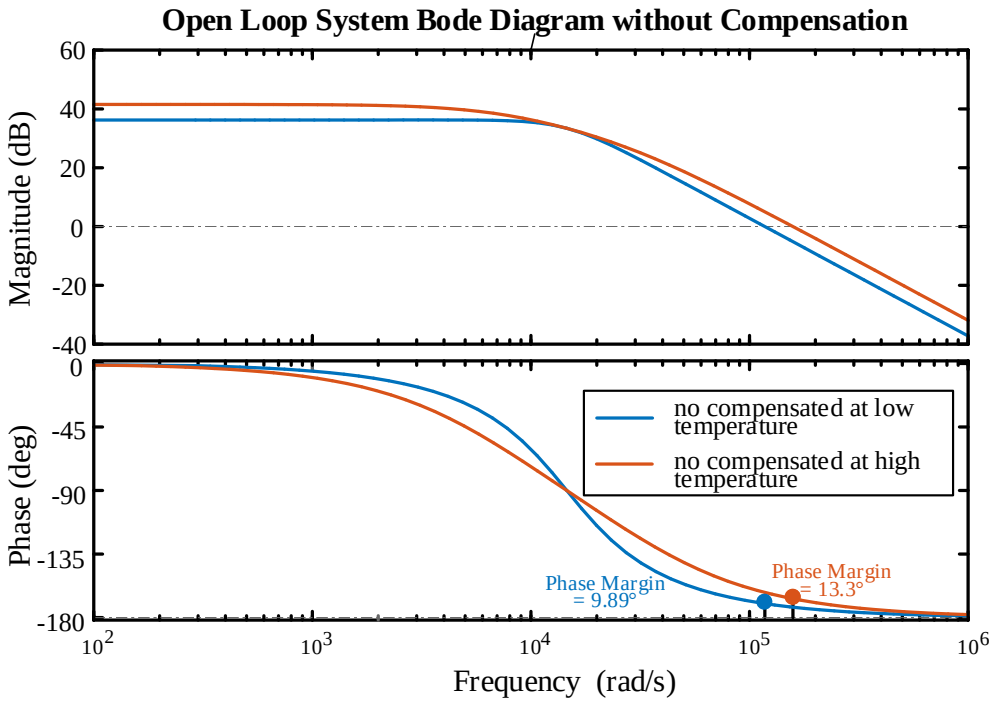

Figure 26 Open Loop system bode plot without compensation

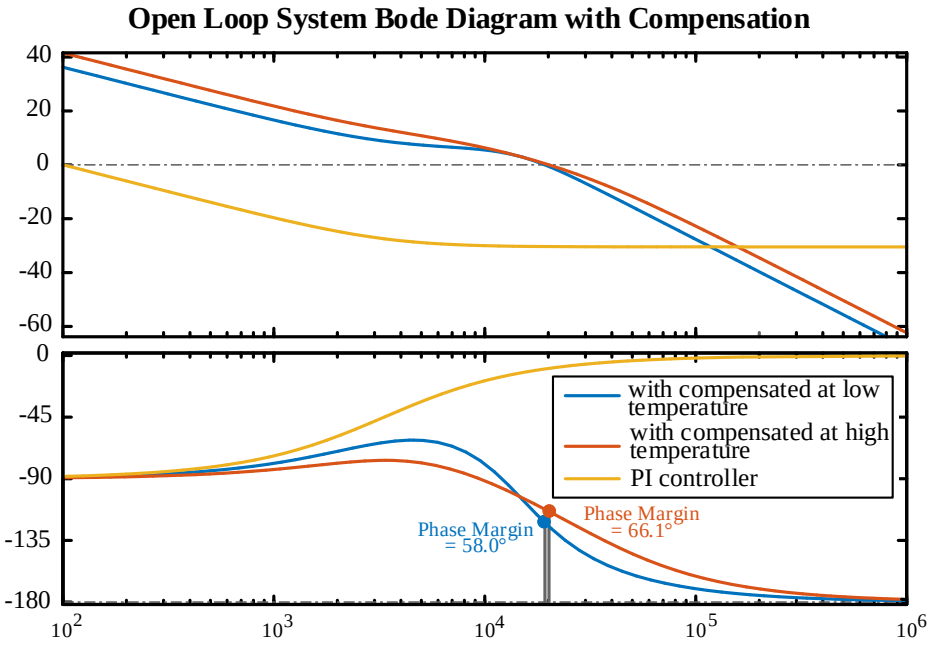

Figure 27 Open Loop system bode plot with compensation

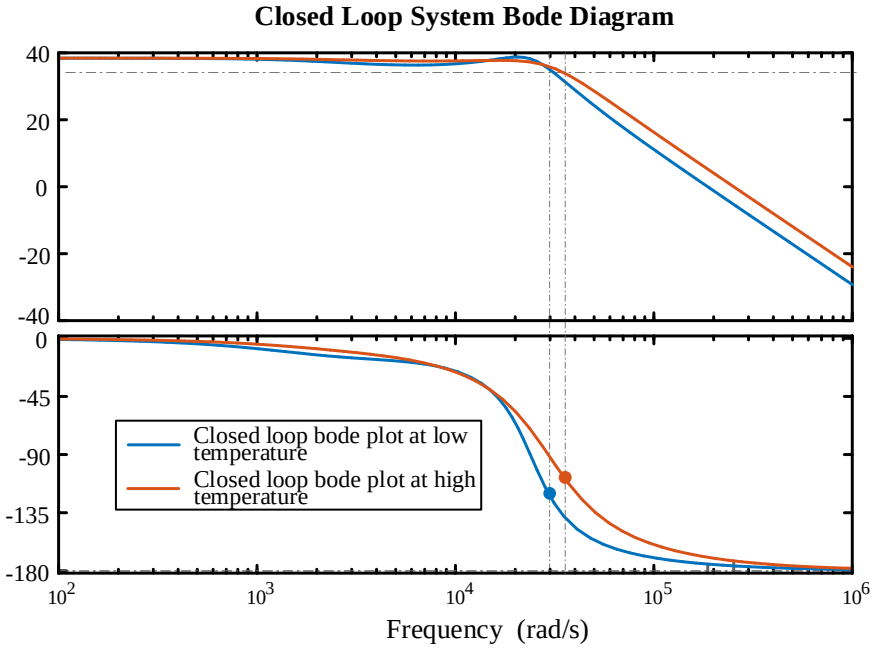

Figure 28 Closed Loop System Bode Diagram

The closed loop body plot shows in Figure 28, the system bandwidth is 4.8 kHz at low temperatures and increases to 5.6 kHz at high temperatures. The bode plot of the thermal dynamic is simulated by solving the thermal network of diode applied with the chosen heatsink. As shown in Figure 29, the bandwidth of thermal dynamic is almost 0. As a result of that, the PA is fast enough for this this T-HIL simulation system.

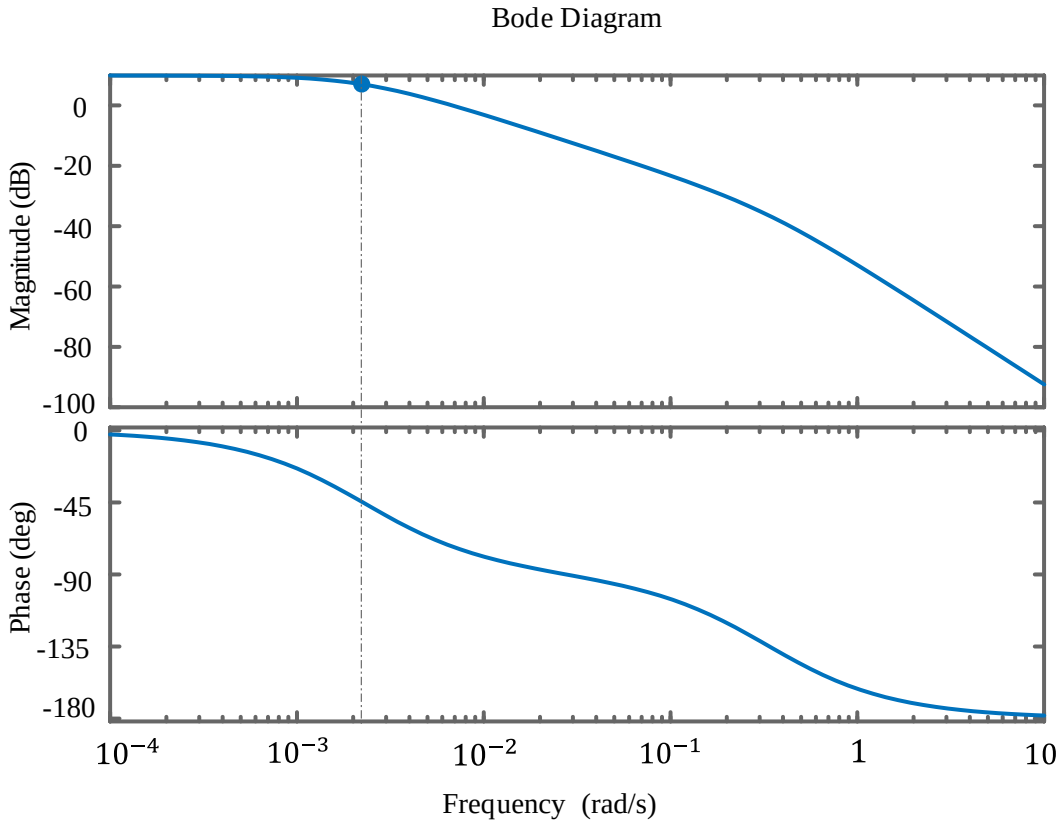

Figure 29 Bode plot of thermal dynamic

Moreover, the experimental measurement of the output power while applying a step function in power reference is shown in Figure 30. It takes about 2.2 seconds for the PA to reach the target power output, which is acceptable in the thermal-based simulation.

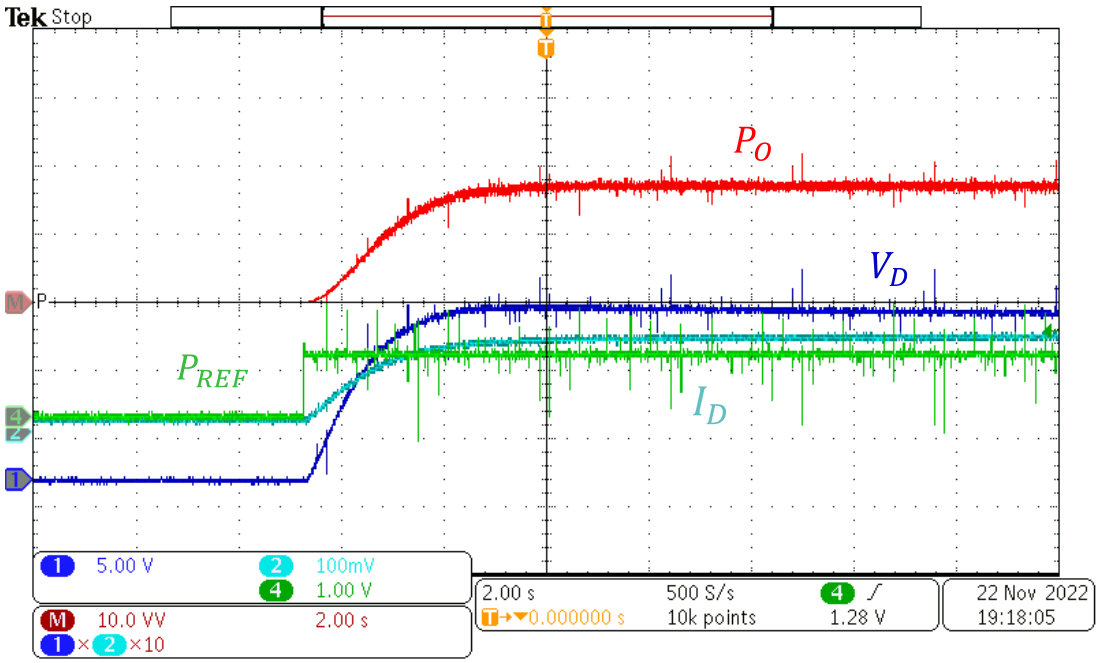

Figure 30 Experimental measurement of output power of PA while applying a step function of power reference

This local controller requires a faster-controlling frequency, at least 10 times faster than the T-HIL system. By taking the advantage of the fast sampling rate of DSP and slow response of temperature, this requirement is achieved successfully. Thus, high-performance FPGA is not necessary for this PA which controls power output to the heating element. For this study, DSP is chosen for its convenience to get in laboratories and higher cost-performance index (CPI).

3.6 Interface accuracy

Analog-to-digital converters (ADC) and Digital-to-Analogue converters (DAC) are essential parts of the communication module between software systems and hardware systems. The communication modules are built in signal level low voltage circuit, measured voltage and current from the power section are required to be scaled first and then sent to input pins of DSP. Very small noise in communication modules can introduce large differences in data processing microcontrollers, as a result of that, insolation between high-voltage power circuits and low-

voltage signal circuits is considerably important. The frequency of sampling process and number of levels in quantization determine the accuracy of the resultant digital signal.

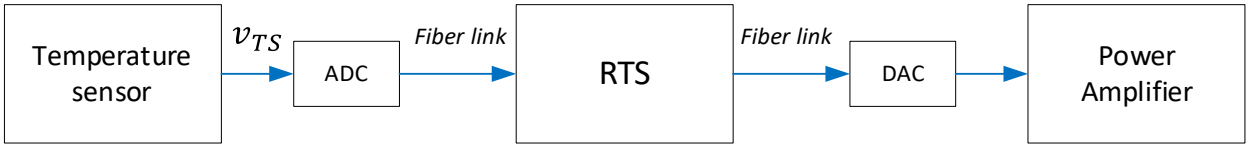

Figure 31 Communication interferences of RTS

In this study, the system has three main communication interfaces: ADC of DSP of power amplifier to receive power reference signal from RSCAD; temperature sensor that measures heatsink surface temperature and sent to RSCAD. Additionally, the accuracy of the temperature sensor that comparing with a digital thermal meter is also examined to ensure the temperature reading is trustable. The above three modules are tested and evaluated individually in the following subsections.

3.6.1 temperature sensor reading

The test for testing the accuracy of the temperature sensor is set up in Figure 32, a FLUKE 52 K/J thermometer is used as the reference. The temperature sensor is mainly built by a monolithic thermocouple amplifier whose output is demonstrated by an oscilloscope through a BNC connector. By taking the advantage of high thermal conductance of liquid, a bottle of water is used as an object with varying temperatures. The water is boiled to ebullition and placed in the paper cup, as the temperature graduate decreasing, measurements of the scope for the temperature sensor and reading from a digital thermometer are taken at the same instance. The comparison is shown

in Figure 33, the straight blue line through the origin represents ideal results of the digital thermometer, and the red square represents the temperature sensor reading (labeled as v_{TS} in Figure 31 and Figure 33). These collected data provide sufficient support that the temperature is accurate enough for measuring the temperature since the dots are very close to the ideal line. The maximum difference between reference temperature and sensor reading is around $1°C$.

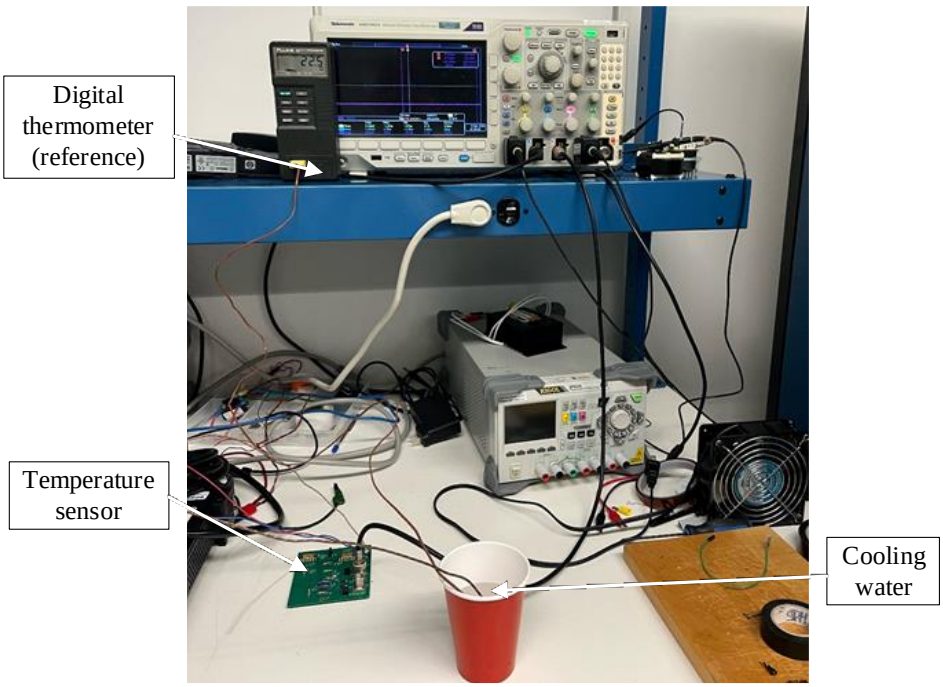

Figure 32 Experimental setup of testing the accuracy of temperature sensor comparing with digital

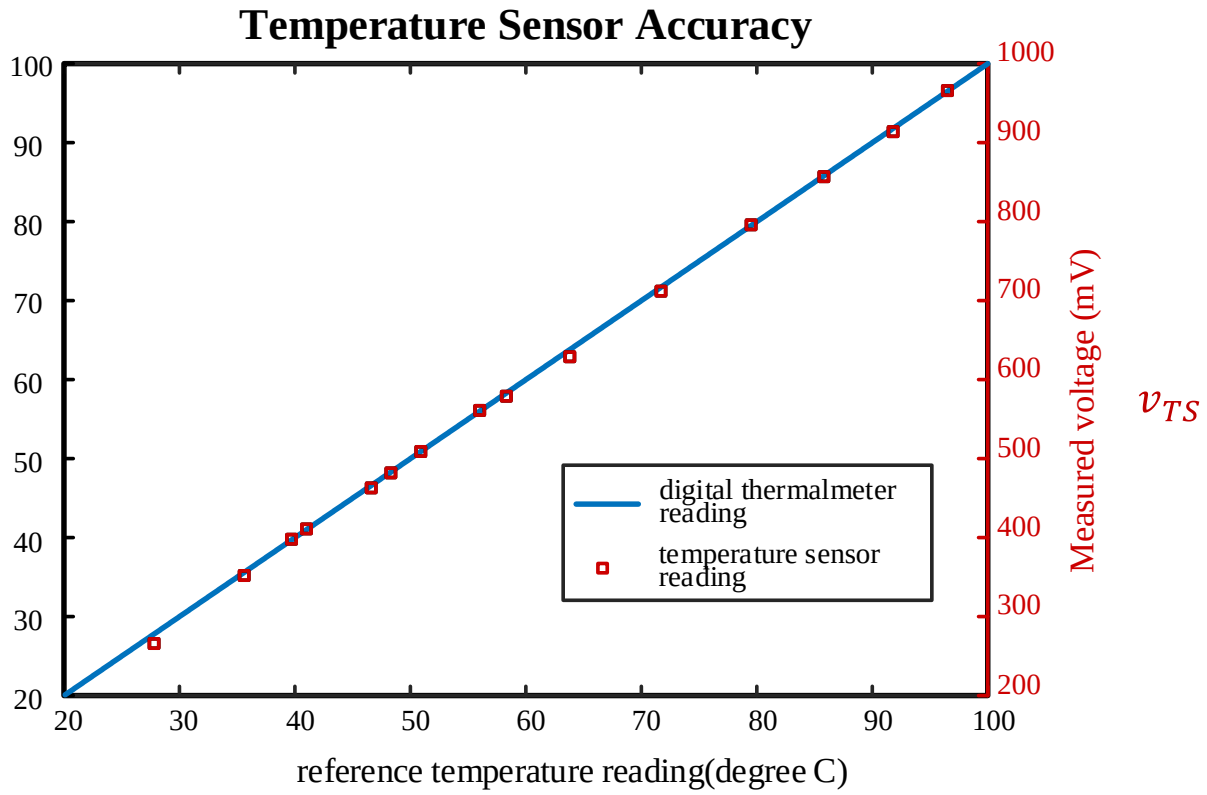

Figure 33 Comparison between digital thermometer and temperature sensor measurements

3.6.3 RSCAD ADC interface accuracy

The embedded ADC module in the RSCAD supercomputer unit is relatively more accurate than the DSP module. The temperature sensor detects the surface temperature on the surface of the heatsink and is sent to the RSCAD machine by signal wire. The conversions of the sensor outputs voltage are low voltage and simple, 10mV equals 1°C. The range of the temperature sensor is from -55°C to 125°C which can cover the whole range of the heatsink in all tests for the chosen diode.

The maximum input voltage for ADC is 10V, thus no additional circuit for scaling the output voltage is required for RSCAD general purpose analog input (GPAI) channel. Digital gain is also introduced in the software module, as shown in Figure 34, by taking the scope measured data as reference labeled as 'ideal reading', the RSCAD reading is roughly on the ideal straight line. This ensures the reading in RSCAD is authentic which further simulation based on is reliable.

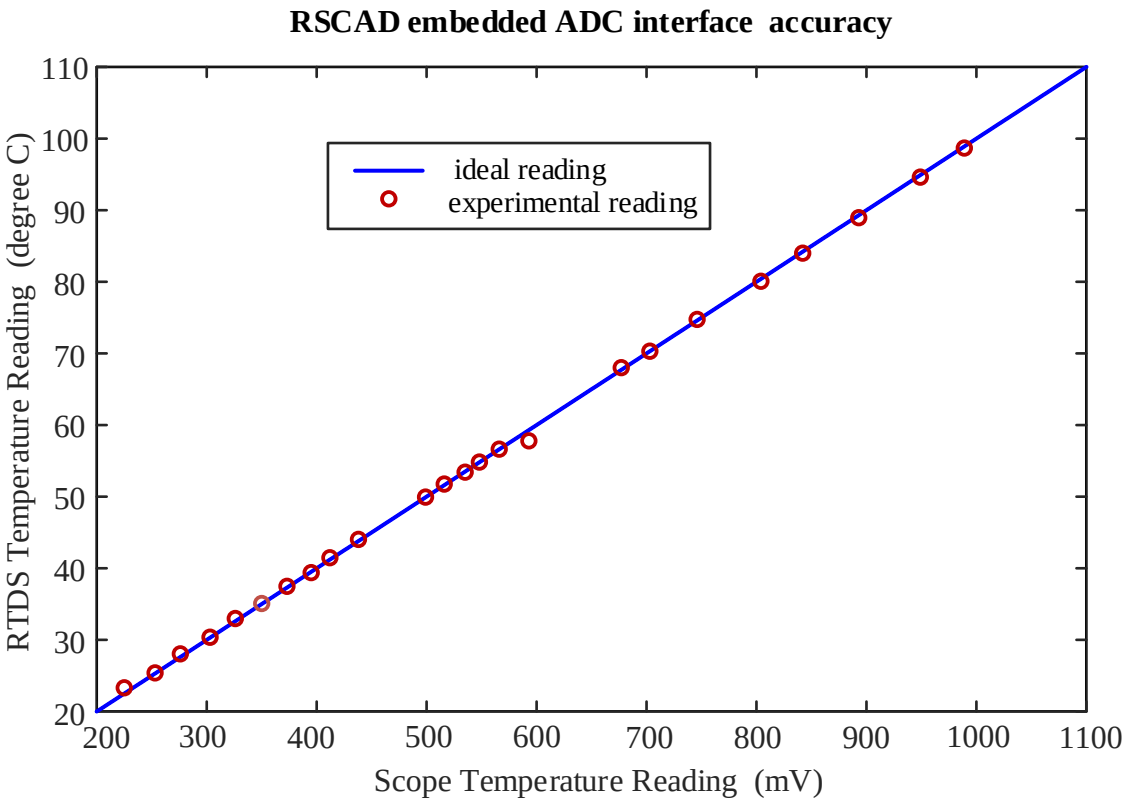

Figure 34 Comparison between temperature sensor data and RSCAD received reading

3.7 Chapter Summary

This chapter comprehensively explains the configuration of each component in the completed system. The switched-mode structure and control strategy of the power amplifier, the algorithm that relocates the current temperature of the working semiconductor, the validation of the diode VIT relationship based on experimental results, and the verification of the digital temperature sensor reading and communication interfaces are all concludes in this chapter. The tested results of each block are shown within the corresponding subsections to provide sufficient support for further open- and closed-loop tests.

Chapter 4 Evaluation

The Thermal-HIL system is implemented in the laboratory as shown in Figure 35 and tested with a heatsink (394-1AB) and PTC (positive temperature coefficient) heater (HP05-1/22-24). The buck converter prototype is programmed by Texas TI™ TMS320F28377S DSP as a power emulator to output a constant power source to the heater. The detailed thermal circuit and diode VIT interpolation module are built inside RSCAD software in RTS (real-time simulation) supercomputer.

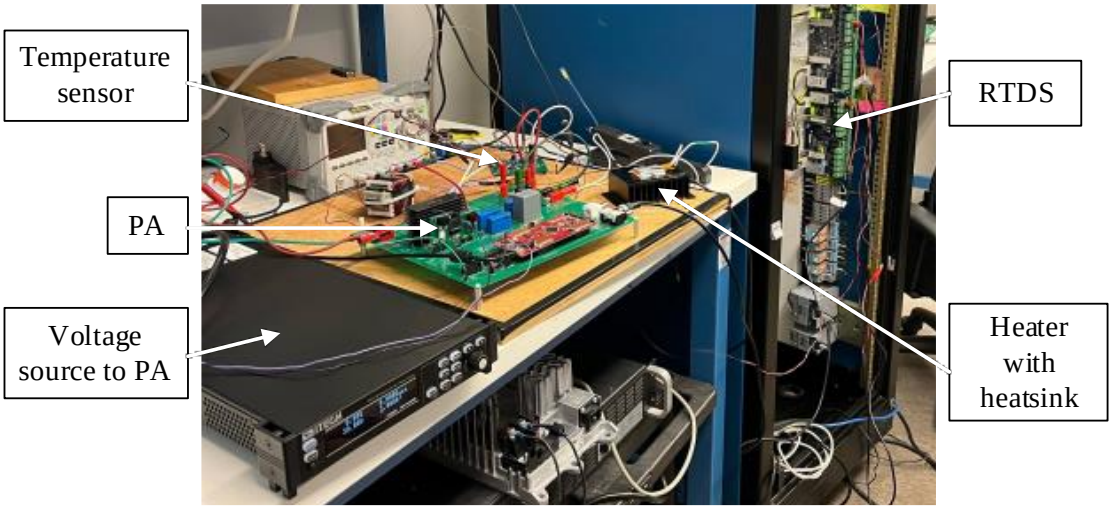

Figure 35 THIL physical set-up

4.1 Open-loop evaluation

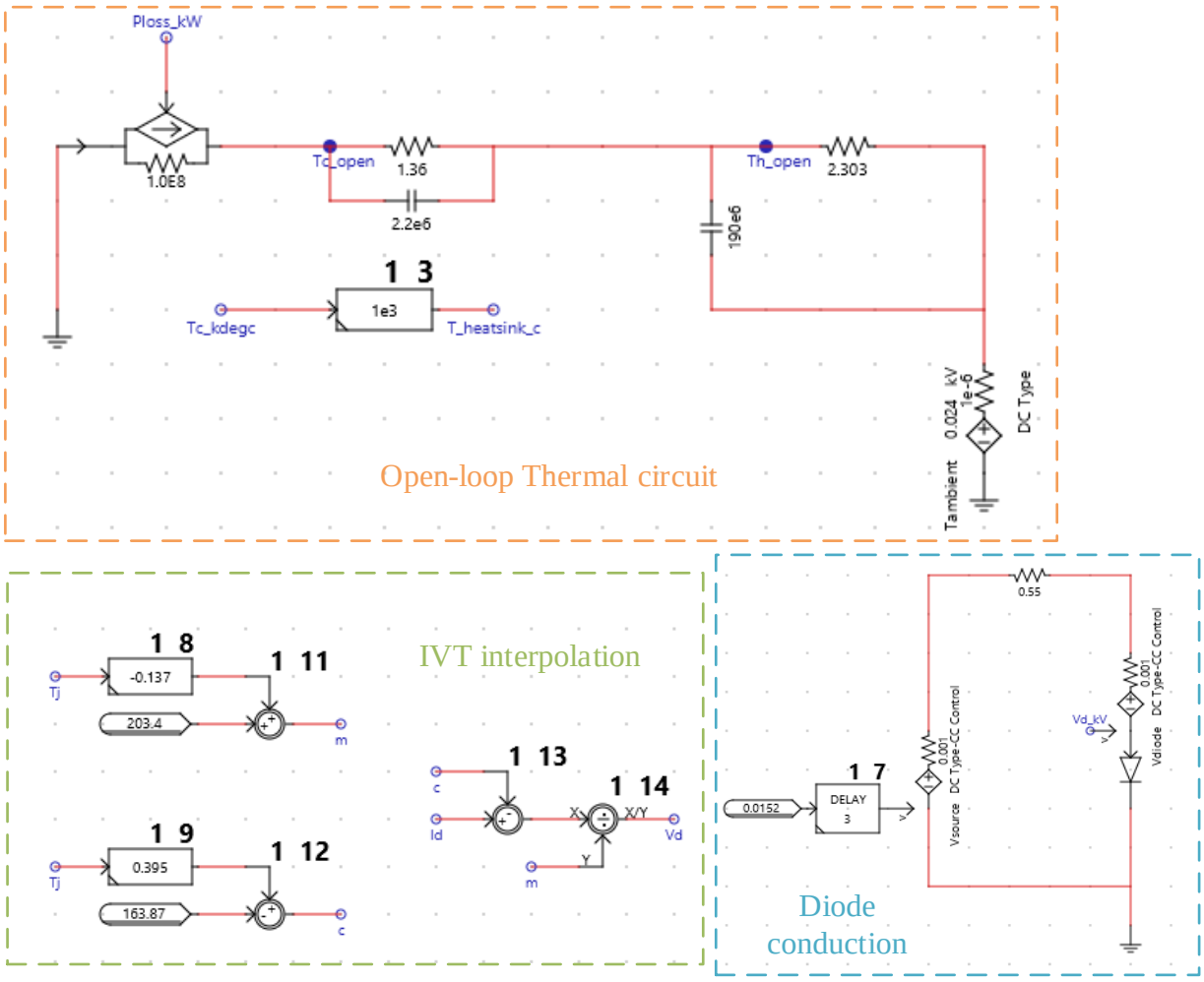

Figure 36 THIL open loop test RSCAD setup

The setup in the software program for the open loop test is shown in Figure 36. In order to verify the heatsink thermal RC network and diode VIT relationship interpolation, the feedback terminal of measurement of heatsink temperature is broken and the room temperature is replaced by a constant voltage source.

Firstly, the performance of the power amplifier is evaluated before closed-loop test. A step

change function of power reference is applied to the power amplifier. The output power (P'_{HS}) and heatsink temperature (T_{HS}) is monitored and the result is shown in Figure 37. A much slower response of temperature rather than a change of power reference is observed. This provides sufficient evidence that PA is able to react fast enough for monitoring dynamic temperature behavior.

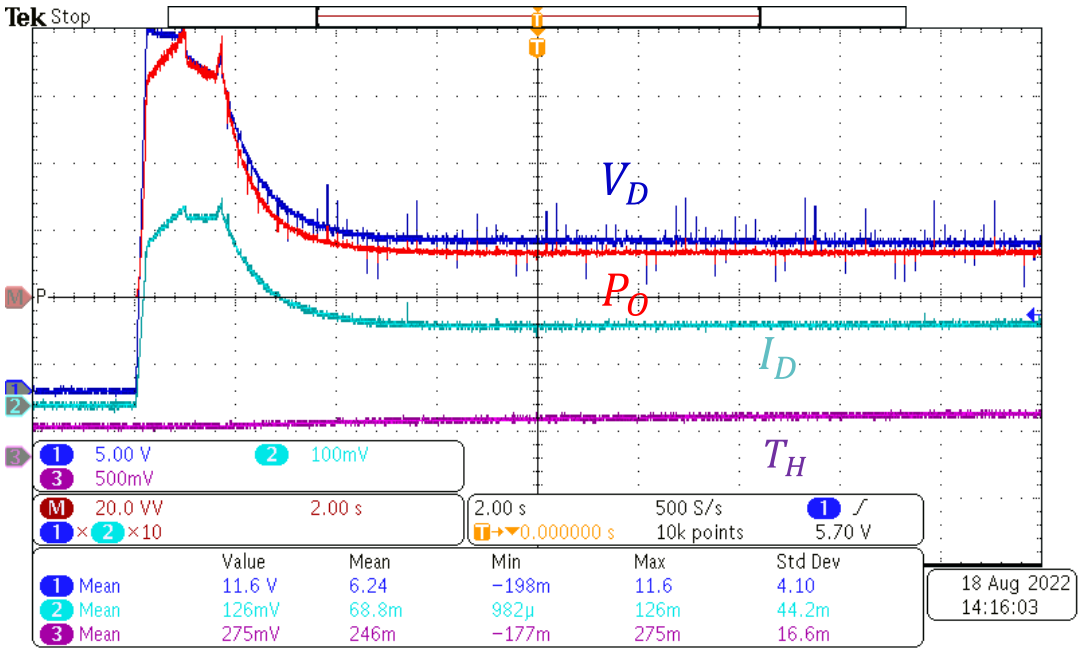

Figure 37 Transient of output power when apply a step function of power reference

Step functions of different power dissipation are applied to both physical diode and software simulation. The same power consumption and room temperature is controlled for each test. The comparison is shown in Figure 38. The matching curve provides sufficient support that the diode IV interpolation and the heatsink thermal model are correct.

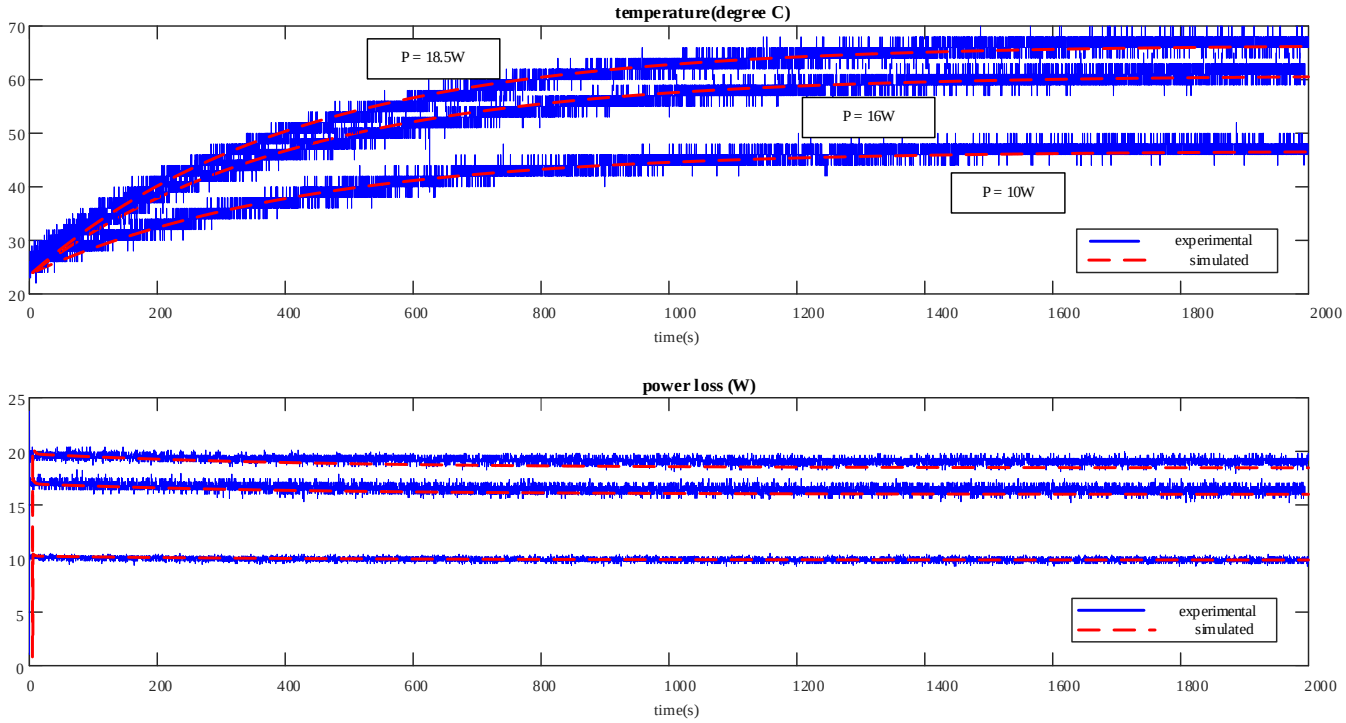

Figure 38 Comparison between software simulation heatsink temperature and physical diode

Then further open loop test is implemented by connecting GPAO (general purpose analog output) to the power amplifier. Calculated diode power consumption in software interpolation is transmitted to PA and generates responding power output to the heating element. Simulation time is enlarged to 4000 seconds to make sure a steady state is reached at end of the simulation. Notice that generally the temperature behavior is matched to the physical diode measurement in three scenarios. Noise is common in measurements and also in DSP analog-to-digital interference, as a result of that, the power output may have a tiny difference in the given power reference value. This can cause steady-state temperature higher, as well as the power output to be higher than physical diode experimental data. The noise gets larger in THIL measurement when output power increases.

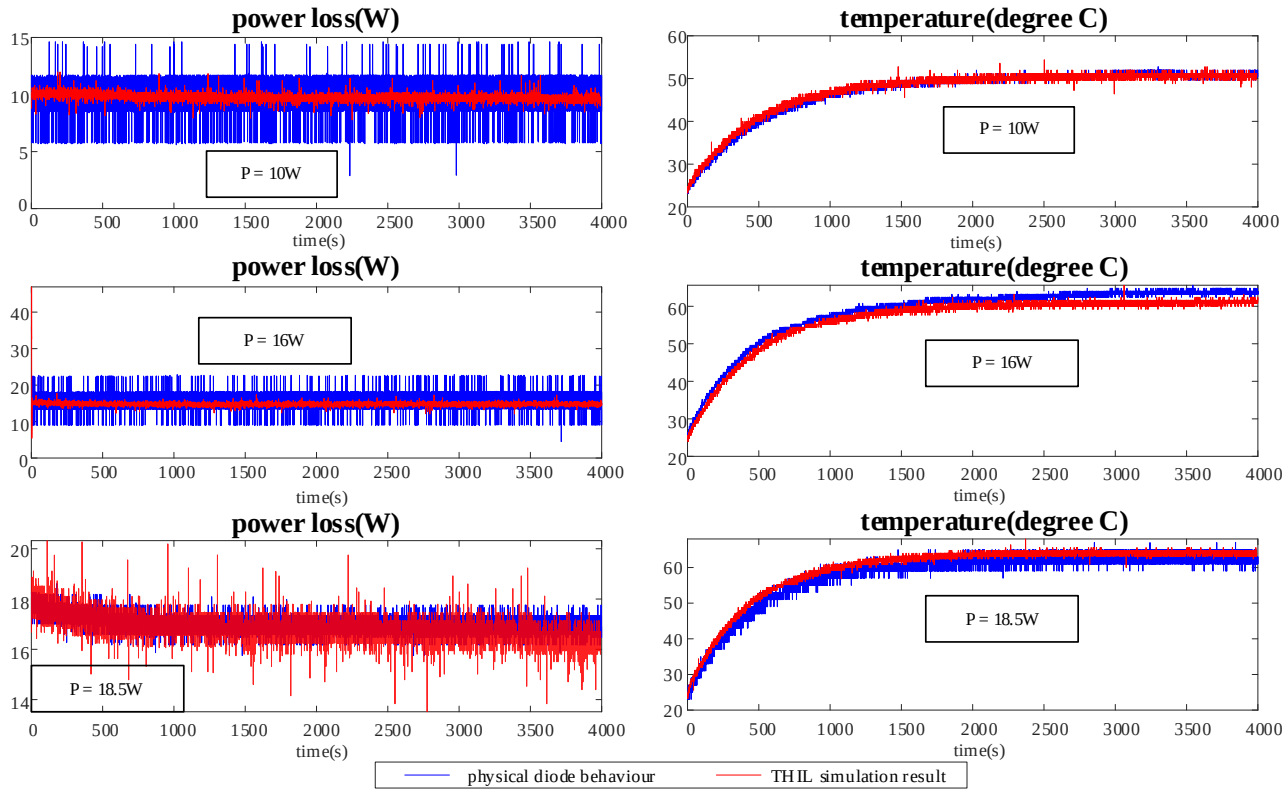

Figure 39 Open loop test by connecting digital power reference to PA at different operating scenarios

4.2 Closed-Loop Evaluation

By connecting the output of the temperature sensor to the GTAI (general purpose analog input) interface of RTS, the closed-loop test is settled. In this case, R_{HA} (heatsink-to-ambient thermal resistance), C_{HA} (heatsink-to-ambient thermal capacitance) section together with the voltage source to represent ambient temperature is replaced by a VCVS (voltage-controlled voltage source). The measured heatsink temperature is scaled back to its real value and sent to the voltage source to heatsink the temperature in the thermal circuit.

Based on verification in the open loop test, the junction temperature is simulated in RSCAD software and compared with the heatsink temperature in Figure 40. Small junction-to-case thermal

capacitance makes the junction temperature follows the same shape as the heatsink temperature. In all scenarios, junction temperatures are within an acceptable range and verifies cooling system choice.

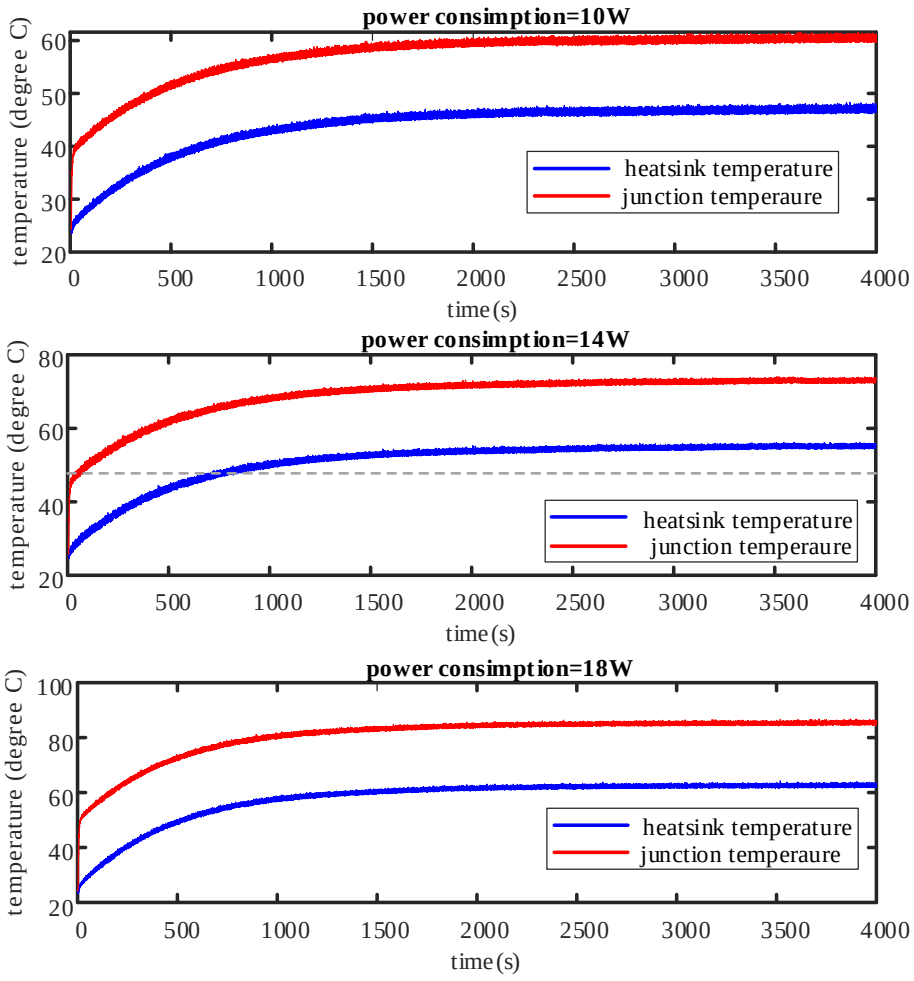

Figure 40 Estimation of diode junction temperature and measured heatsink temperature at different power dissipation conditions

Chapter 5 Conclusion and Future Work

5.1 Conclusion

This thesis fabricated a real-time evaluation platform of cooling systems, which is based on Thermal-Hardware-In-the-Loop methodology for power electronics under different operation conditions.

System-level evaluation is set up in laboratory for open-loop and closed-loop tests. The heatsink thermal RC parameters and diode IV characteristic model are verified by open-loop simulation results. The measured heatsink surface temperature and comparison with the physical diode behavior agree with each other.

After replacing the heatsink RC section with a VCVS in the thermal circuit, the closed-loop test is settled. Based on the substantiated results from open-loop test, the closed-loop test emulates the junction temperature of conducting diode at different power consumption. In all scenarios, the steady-state junction temperatures of the diode are maintained with an acceptable working range, which verifies the choice of heatsink as DUT. Additionally, the tested environment can be easily changed in the software program, which allows tests in more crucial conditions that are close to maximum value without worrying about damaging the actual component.

5.2 Future Work

Further study can be expected to be applied in high-frequency power converters with more complicated circuits. In high-frequency scenarios, the case will be more complicated since a larger number of semiconductors are in operation. Both conduction and switching loss related to switching transient will be taken into consideration. More physical tests to determine the mathematical modules of semiconductor loss are required.

Meanwhile, the semiconductors normally are located very close to each other, mutual temperature interaction makes significant influence on determining the semiconductor junction temperature. This impact relates to distance, heat energy dissipation, and other environmental conditions. Related studies to all the mentioned parameters and senarios are expected in the future.

Reference

[1] C. Pica, R. Bojoi, G. Griva and A. Tenconi, "Series-connected DC-DC power converters for low-voltage dc source in distributed generation," 2007 9th International Conference on Electrical Power Quality and Utilisation, 2007, pp. 1-6, doi: 10.1109/EPQU.2007.4424173.

[2] S. Ming-ming, Z. Bo and W. Jia-dan, "Simulation research on a novel distributed generation system," 2011 4th International Conference on Power Electronics Systems and Applications, 2011, pp. 1-5, doi: 10.1109/PESA.2011.5982941.

[3] Y. Zhu, S. Shi, F. Wang, F. Zhuo, S. Cheng and H. Yi, "Quasi Square Wave Modulation With Voltage Transformation Ability Applied to Modular Multilevel DC-DC Converter," 2018 IEEE Energy Conversion Congress and Exposition (ECCE), 2018, pp. 3050-3054, doi: 10.1109/ECCE.2018.8557397.

[4] Z. Guo, H. Li, C. Liu, Y. Zhao and W. Su, "Stability-improvement method of cascaded DC-DC converters with additional voltage-error mutual feedback control," in Chinese Journal of Electrical Engineering, vol. 5, no. 2, pp. 63-71, June 2019, doi: 10.23919/CJEE.2019.000012.

[5] B. Singh, V. Garg and G. Bhuvaneswari, "Polygon Connected 15-Phase AC-DC Converter for Power Quality Improvement," 2006 International Conference on Power Electronic, Drives and Energy Systems, 2006, pp. 1-5, doi: 10.1109/PEDES.2006.344245.

[6] B. Singh, V. Garg and G. Bhuvaneswari, "Power Quality Improvements Using Delta-Polygon Connected Autotransformer Based Nine Phase AC-DC Converter," 2006 IEEE International Conference on Industrial Technology, 2006, pp. 2719-2724, doi: 10.1109/ICIT.2006.372603.

[7] Y. Kusuhara, A. Nakayama, T. Ninomiya and S. Nakagawa, "Power Flow Control for Efficiency Improvement in a Forward-Flyback Mixed Converter," 2007 7th International Conference on Power Electronics and Drive Systems, 2007, pp. 749-753, doi: 10.1109/PEDS.2007.4487787.

[8] B. K. Lee, J. P. Hong and M. Ehsani, "Generalized design methodology of reduced parts converters for low cost BLDC motor drives," Eighteenth Annual IEEE Applied Power Electronics Conference and Exposition, 2003. APEC '03., 2003, pp. 277-280 vol.1, doi: 10.1109/APEC.2003.1179226.

[9] S. K. Tso and C. S. Chan, "A Low-Cost Microcontroller-Based AC/DC Converter with Improved Power Factor," Proceedings.14 Annual Conference of Industrial Electronics Society, 1988, pp. 848-852, doi: 10.1109/IECON.1988.665833.

[10] P. Julian, A. Oliva, P. Mandolesi and H. Chiacchiarini, "Output discrete feedback control of a DC-DC buck converter," ISIE '97 Proceeding of the IEEE International Symposium on Industrial Electronics, 1997, pp. 925-930 vol.3, doi: 10.1109/ISIE.1997.648847.

[11] B. Bryant and M. K. Kazimierezuk, "Derivation of the buck-boost PWM DC-DC converter circuit topology," 2002 IEEE International Symposium on Circuits and Systems (ISCAS), 2002, pp. V-V, doi: 10.1109/ISCAS.2002.1010835.

[12] R. Philip and C. Sreeja, "Single phase PFC using Buck-Boost converter," 2014 Annual International Conference on Emerging Research Areas: Magnetics, Machines and Drives (AICERA/iCMMD), 2014, pp. 1-5, doi: 10.1109/AICERA.2014.6908174.

[13] T. W. Martin and S. S. Ang, "Digital control for switching converters," 1995 Proceedings of the IEEE International Symposium on Industrial Electronics, 1995, pp. 480-484 vol.2, doi: 10.1109/ISIE.1995.497232.

[14] K. Jezernik, "FPGA-based controllers for switching converters," IEEE EUROCON 2009, 2009, pp. 971-976, doi: 10.1109/EURCON.2009.5167752.

[15] Bo Huang, "Design and implementation of multi-channel digital down-converter based on DSP," Proceedings of 2011 International Conference on Computer Science and Network Technology, 2011, pp. 1846-1850, doi: 10.1109/ICCSNT.2011.6182329.

[16] "White paper: FPGA VS. DSP Design Reliability and Maintenance", Intel.com, 2007. [Online].Available:https://www.intel.com/content/dam/support/us/en/programmable/support-resources/bulk-container/pdfs/literature/wp/wp-01023.pdf. [Accessed: 31- Aug- 2022].

[17] R. Zaheri and J. Shokrollahi Moghani, "A Modular Two-Stage High Step-Down DC-DC Converter Using Frequency Multiplier Circuit for Datacenter Applications," 2021 12th Power Electronics, Drive Systems, and Technologies Conference (PEDSTC), 2021, pp. 1-5, doi: 10.1109/PEDSTC52094.2021.9405950.

[18] V. V. N. Obreja, "The semiconductor - dielectric interface from PN junction periphery and its influence on reliability of power devices at high temperature," 2008 14th International Workshop on Thermal Inveatigation of ICs and Systems, 2008, pp. 142-147, doi: 10.1109/THERMINIC.2008.4669896.

[19] M. S. Abadir, K. Khouri and A. Gupta, "Temperature aware SoC design for reduced leakage power and enhanced reliability," 2008 IEEE International Symposium on VLSI Design, Automation and Test (VLSI-DAT), 2008, pp. 4-4, doi: 10.1109/VDAT.2008.4542398.

[20] A. Nakagawa, H. Ohashi, M. Kurata, H. Yamaguchi and K. Watanabe, "Non-latch-up 1200V 75A bipolar-mode MOSFET with large ASO," 1984 International Electron Devices Meeting, 1984, pp. 860-861, doi: 10.1109/IEDM.1984.190866.

[21] Kahng, Dawon, "Electric Field Controlled Semiconductor Device," U. S. Patent No. 3,102,230 (Filed 31 May 31, 1960, issued August 27, 1963).

[22] W. Lee, D. Han, C. Morris and B. Sarlioglu, "Minimizing switching losses in high switching frequency GaN-based synchronous buck converter with zero-voltage resonant-transition switching," 2015 9th International Conference on Power Electronics and ECCE Asia (ICPE-ECCE Asia), 2015, pp. 233-239, doi: 10.1109/ICPE.2015.7167792.

[23] P. Sojka, M. Pipiska and M. Frivaldsky, "GaN power transistor switching performance in hard-switching and soft-switching modes," 2019 20th International Scientific Conference on Electric Power Engineering (EPE), 2019, pp. 1-5, doi: 10.1109/EPE.2019.8778060.

[24] R. Maier, P. Friedrichs, G. Griepentrog and M. Schroeck, "Modeling of silicon carbide (SiC) power devices for electronic switching in low voltage applications," 2004 IEEE 35th

Annual Power Electronics Specialists Conference (IEEE Cat. No.04CH37551), 2004, pp. 2742-2745 Vol.4, doi: 10.1109/PESC.2004.1355266.

[25] D. Goldmann, S. Mayer, S. Schramm and H. -G. Herzog, "Comparing Switching and Conduction Losses of Uni- and Bidirectional SiC Semiconductor Switches for AC Applications," 2021 23rd European Conference on Power Electronics and Applications (EPE'21 ECCE Europe), 2021, pp. P.1-P.9, doi: 10.23919/EPE21ECCEEurope50061.2021.9570496. xxx.

[26] K. Berringer, J. Marvin and P. Perruchoud, "Semiconductor power losses in AC inverters," IAS '95. Conference Record of the 1995 IEEE Industry Applications Conference Thirtieth IAS Annual Meeting, 1995, pp. 882-888 vol.1, doi: 10.1109/IAS.1995.530391.

[27] H. Dong, C. Zhang and C. Hu, "Effect of switching frequency and floating capacitor for five-level inverter," 2018 13th IEEE Conference on Industrial Electronics and Applications (ICIEA), 2018, pp. 1476-1480, doi: 10.1109/ICIEA.2018.8397942.

[28] K. Matocha, P. Losee, J. Glaser, J. Nasadoski, S. Arthur and L. Stevanovic, "Getting the most from SiC MOSFETs: Optimizing conduction and switching losses for high performance power electronics applications," 2009 International Semiconductor Device Research Symposium, 2009, pp. 1-2, doi: 10.1109/ISDRS.2009.5378062.

[29] Z. Chen, "An inductive-switching loss model accounting for source inductance and switching loop inductance," 2014 IEEE Applied Power Electronics Conference and Exposition - APEC 2014, 2014, pp. 497-504, doi: 10.1109/APEC.2014.6803355.

[30] Y. Shen, J. Jiang, Y. Xiong, Y. Deng, X. He and Z. Zeng, "Parasitic Inductance Effects on the Switching Loss Measurement of Power Semiconductor Devices," 2006 IEEE International Symposium on Industrial Electronics, 2006, pp. 847-852, doi: 10.1109/ISIE.2006.295745.

[31] J. W. Sofia, "Analysis of thermal transient data with synthesized dynamic models for semiconductor devices," in IEEE Transactions on Components, Packaging, and

Manufacturing Technology: Part A, vol. 18, no. 1, pp. 39-47, March 1995, doi: 10.1109/95.370733.

[32] S. Munk-Nielsen, L. N. Tutelea and U. Jaeger, "Simulation with ideal switch models combined with measured loss data provides a good estimate of power loss," Conference Record of the 2000 IEEE Industry Applications Conference. Thirty-Fifth IAS Annual Meeting and World Conference on Industrial Applications of Electrical Energy (Cat. No.00CH37129), 2000, pp. 2915-2922 vol.5, doi: 10.1109/IAS.2000.882580.xxx

[33] G. Feix, S. Dieckerhoff, J. Allmeling and J. Schonberger, "Simple methods to calculate IGBT and diode conduction and switching losses," 2009 13th European Conference on Power Electronics and Applications, 2009, pp. 1-8.

[34] S. S. Ahmad and G. Narayanan, "Double pulse test based switching characterization of SiC MOSFET," 2017 National Power Electronics Conference (NPEC), 2017, pp. 319-324, doi: 10.1109/NPEC.2017.8310478.

[35] A. Ghosh, C. N. M. Ho, J. Prendergast and Y. Xu, "Conceptual Design and Demonstration of an Automatic System for Extracting Switching Loss and Creating Data Library of Power Semiconductors," in IEEE Open Journal of Power Electronics, vol. 1, pp. 431-444, 2020, doi: 10.1109/OJPEL.2020.3026896.

[36] Y. Zhu, K. Ma and G. Konstantinou, "Loss and Thermal Characterization Methods for Power Semiconductor Devices Based on H-bridge Circuit," 2020 IEEE 9th International Power Electronics and Motion Control Conference (IPEMC2020-ECCE Asia), 2020, pp. 3465-3469, doi: 10.1109/IPEMC-ECCEAsia48364.2020.9368230.

[37] Z. Guo, G. Cao and Y. Wang, "A novel semiconductor switch test platform for power converter optimization," 2017 20th International Conference on Electrical Machines and Systems (ICEMS), 2017, pp. 1-4, doi: 10.1109/ICEMS.2017.8056144.

[38] A. Bar-Cohen and M. Iyengar, "Design and optimization of air-cooled heat sinks for sustainable development," in IEEE Transactions on Components and Packaging Technologies, vol. 25, no. 4, pp. 584-591, Dec. 2002, doi: 10.1109/TCAPT.2003.809112.

[39] M. L. McGeary, "Integral heatsink polysilicon semiconductor packaging," 1992 Proceedings 42nd Electronic Components & Technology Conference, 1992, pp. 807-813, doi: 10.1109/ECTC.1992.204299.

[40] H. Beiranvand, E. Rokrok and M. Liserre, "Comparative Study of Heatsink Volume and Weight Optimization in SST DAB cells Employing GaN, SiC-MOSFET and Si-IGBT Switches," 2019 10th International Power Electronics, Drive Systems and Technologies Conference (PEDSTC), 2019, pp. 297-302, doi: 10.1109/PEDSTC.2019.8697276.

[41] A. Jain, R. E. Jones, Ritwik Chatterjee, S. Pozder and Zhihong Huang, "Thermal modeling and design of 3D integrated circuits," 2008 11th Intersociety Conference on Thermal and Thermomechanical Phenomena in Electronic Systems, 2008, pp. 1139-1145, doi: 10.1109/ITHERM.2008.4544389.

[42] H. Zhao, J. Lv, M. Liu and X. Ren, "Simulation and Optimization Analysis of Vehicle Cooling System," 2021 4th World Conference on Mechanical Engineering and Intelligent Manufacturing (WCMEIM), 2021, pp. 493-497, doi: 10.1109/WCMEIM54377.2021.00106.

[43] F. Song, Jiayi Yuan, Xindong Tian and Guobiao Gu, "Development of high gradient magnetic filter with evaporative cooling system," 2008 International Conference on Electrical Machines and Systems, 2008, pp. 708-711.

[44] K. Radhakrishnan, D. Wittwer and Yuan-Liang Li, "Study of heatsink grounding schemes for GHz microprocessors," IEEE 9th Topical Meeting on Electrical Performance of Electronic Packaging (Cat. No.00TH8524), 2000, pp. 189-192, doi: 10.1109/EPEP.2000.895525.

[45] P. Zhang, X. Qiu, Z. Zheng, G. fu, S. Duan and Y. Zhang, "Comparison of the Water-cooling System and the Liquid-metal-cooling System for hybrid HVDC Circuit Breakers," 2019 2nd International Conference on Information Systems and Computer Aided Education (ICISCAE), 2019, pp. 131-134, doi: 10.1109/ICISCAE48440.2019.221603.

[46] Shuke Li, Guoqiang Zhang, Hui Guo, Fuchuan Song, Jiayi Yuan and Guobiao Gu, "The application of evaporative cooling technology for an electromagnetic separator," 2005 International Conference on Electrical Machines and Systems, 2005, pp. 1767-1770 Vol. 3, doi: 10.1109/ICEMS.2005.202863.

[47] J. Li, F. Song, G. Gu and X. Tian, "Experimental invetigation on air-cooling condenser in close-loop self-circulating evaporative cooling system of large electrical equipments," 2009 International Conference on Electrical Machines and Systems, 2009, pp. 1-5, doi: 10.1109/ICEMS.2009.5382677.

[48] I. Tari and F. S. Yalcin, "CFD Analyses of a Notebook Computer Thermal Management System and a Proposed Passive Cooling Alternative," in IEEE Transactions on Components and Packaging Technologies, vol. 33, no. 2, pp. 443-452, June 2010, doi: 10.1109/TCAPT.2010.2044505.

[49] S. A. Kale, Y. R. Gunjal, S. P. Jadhav and A. N. Tanksale, "CFD analysis for optimization of diffuser for a micro wind turbine," 2013 International Conference on Energy Efficient Technologies for Sustainability, 2013, pp. 257-260, doi: 10.1109/ICEETS.2013.6533392.

[50] T. Konishi, R. Kibushi, T. Hatakeyama, S. Nakagawa and M. Ishizuka, "Evaluation of Amount of Heat Through Each Component of SiC Package Using CFD Analysis," 2022 International Conference on Electronics Packaging (ICEP), 2022, pp. 111-112, doi: 10.23919/ICEP55381.2022.9795488.

[51] John Turner, "1. Characterizing Thermal Behavior of an Air-Cooled Lithium-Ion Battery System for HEV Applications Using FEA Approach (2013-01-1520)," in Progress in Modeling and Simulation of Batteries , SAE, 2016, pp.3-11.

[52] T. Wu, Z. Wang, B. Ozpineci, M. Chinthavali and S. Campbell, "Automated Heatsink Optimization for Air-Cooled Power Semiconductor Modules," in IEEE Transactions on Power Electronics, vol. 34, no. 6, pp. 5027-5031, June 2019, doi: 10.1109/TPEL.2018.2881454.

[53] H. P. de Bock, "Exploration of a Hybrid Analytical Thermal Topology Optimization Method for an Additively Manufactured Heat Sink," 2018 17th IEEE Intersociety Conference on Thermal and Thermomechanical Phenomena in Electronic Systems (ITherm), 2018, pp. 761-767, doi: 10.1109/ITHERM.2018.8419585.

[54] S. K. Jain, C. Ameta and G. Narayanan, "Real-time simulation of IEEE 3-generator 9-bus system on miniature full spectrum simulator," 2017 National Power Electronics Conference (NPEC), 2017, pp. 246-251, doi: 10.1109/NPEC.2017.8310466.

[55] A. Perić, H. Pauković, M. Miletić and V. Šunde, "Development of voltage source converter using HiL simulation system," 2019 42nd International Convention on Information and Communication Technology, Electronics and Microelectronics (MIPRO), 2019, pp. 168-173, doi: 10.23919/MIPRO.2019.8757020.

[56] Luca, L. Condrachi, L. Luca, R. Vilanova and M. Barbu, "Testing Platform for Real-Time Controllers Based on Hardware In the Loop Simulation," 2021 26th IEEE International Conference on Emerging Technologies and Factory Automation (ETFA), 2021, pp. 1-4, doi: 10.1109/ETFA45728.2021.9613263.

[57] Y. Huo, G. Gruosso and L. Piegari, "Power hardware in the loop simulator of photovoltaic plant for smart grid interation analysis," 2017 IEEE International Conference on Environment and Electrical Engineering and 2017 IEEE Industrial and Commercial Power Systems Europe (EEEIC / I&CPS Europe), 2017, pp. 1-5, doi: 10.1109/EEEIC.2017.7977629.

[58] RTDS Technologies, “Flexible, scalable I/O over copper or Ethernet,” SIMULATION HARDWARE. https://www.rtds.com/technology/simulation-hardware/ (accessed Oct. 11, 2022).

[59] C. N. M. Ho, Y. Fang, Y. Xu, and I. Jayawardana, "Thermal-HIL Real-Time Testing Platform for Evaluating Cooling Systems of Power Rectifiers," 2021 IEEE Energy Conversion Congress and Exposition (ECCE), 2021, pp. 5729-5734, doi: 10.1109/ECCE47101.2021.9595363.

[60] Y. C. Gerstenmaier, W. Kiffe and G. Wachutka, "Combination of thermal subsystems modeled by rapid circuit transformation," 2007 13th International Workshop on Thermal Investigation of ICs and Systems (THERMINIC), 2007, pp. 115-120, doi: 10.1109/THERMINIC.2007.4451758.

[61] K. Ma, N. He, M. Liserre and F. Blaabjerg, "Frequency-Domain Thermal Modeling and Characterization of Power Semiconductor Devices," in IEEE Transactions on Power Electronics, vol. 31, no. 10, pp. 7183-7193, Oct. 2016, doi: 10.1109/TPEL.2015.2509506.